

# Spectral classification of one-dimensional binary aperiodic crystals : An algebraic approach

Enrique Maciá

*Dpto. Física de Materiales, Facultad CC. Físicas,  
Universidad Complutense de Madrid, E-28040, Spain*

(Dated: May 31, 2017)

## Abstract

A spectral classification of general one-dimensional binary aperiodic crystals (BACs) based on both their diffraction patterns and energy spectrum measures is introduced along with a systematic comparison of the zeroth-order energy spectrum main features for BACs belonging to different spectral classes, including Fibonacci-class, precious means, metallic means, mixed means and period doubling based representatives. These systems are described by means of mixed-type Hamiltonians which include both diagonal and off-diagonal terms aperiodically distributed. An algebraic approach highlighting chemical correlation effects present in the underlying lattice is introduced. Close analytical expressions are obtained by exploiting some algebraic properties of suitable blocking schemes preserving the atomic order of the original lattice. The existence of a resonance energy which defines the basic anatomy of the zeroth-order energy spectra structure for the standard Fibonacci, the precious means and the Fibonacci-class quasicrystals is disclosed. This eigenstate is also found in the energy spectra of BACs belonging to other spectral classes, but for specific particular choices of the corresponding model parameters only. The transmission coefficient of these resonant states is always bounded below, although their related Landauer conductance values may range from highly conductive to highly resistive ones, depending on the relative strength of the chemical bonds.

## INTRODUCTION

In 1992 the International Union of Crystallography widened the very definition of crystal, distinguishing between periodic and *aperiodic* crystals, respectively.[1] The revamped crystal definition reflects our current understanding that atomic periodicity is a sufficient but not necessary condition for crystallinity, and that the presence of an appropriate *long-range* atomic order, rendering discrete diffraction patterns, must be regarded as the proper *generic* attribute of crystalline matter. Up to date, three main families of aperiodic crystals have been identified, namely, incommensurate modulated phases, incommensurate composites and quasicrystals.[2–4] Quasiperiodic crystals (QCs) can be regarded as a natural extension of the periodic crystal concept to structures where periodic translation symmetry is replaced by a richer long-range order described in terms of more general quasiperiodic functions instead.[5]

A key question in any general theory of aperiodic crystals regards the relationship between their atomic spatial order, determined by a given aperiodic distribution of atoms *and* bonds, and the physical properties stemming from that structure. In particular, since the electronic structure of a solid depends on both the spatial distribution of its constituent atoms and their bonding properties one may reasonably expect that aperiodic crystals belonging to different structural classes would exhibit some characteristic distinctive features in their electronic structures as well. From the view point of condensed matter physics there are two important spectral measures one can consider when studying the properties of solid materials. On the one hand, we have a measure related to the atomic density distribution Fourier transform, which discloses the main features of X-ray, electron or neutron diffraction patterns resulting from the spatial structure of the solid. On the other hand, we have a measure related to the energy (frequency) spectra of the system, describing its electronic structure (or the frequency distribution of the atomic vibrations in the case of the phonon spectrum). According to Lebesgue’s decomposition theorem both measures can be uniquely decomposed in terms of three kinds of spectral components (and mixtures of them), namely: pure point ( $\mu_P$ ), absolutely continuous ( $\mu_{AC}$ ) and singularly continuous ( $\mu_{SC}$ ) spectra, in the form  $\mu = \mu_P \cup \mu_{AC} \cup \mu_{SC}$ . [6, 7]

In order to gain a deeper insight on the relationship between the structural order present in an aperiodic solid (as determined by its diffraction pattern) and its related transport

<b>ENERGY SPECTRUM</b>	$\mu_{AC}$	<b>PERIODIC CRYSTALS</b>		<b>VOGEL SPIRAL LATTICES</b>
	$\mu_{SC}$	<b>FIBONACCI PERIOD-DOUBLING</b>	<b>THUE-MORSE NICKEL MEAN</b>	<b>RUDIN-SHAPIRO?</b>
	$\mu_P$	<b>IDEAL QUASICRYSTAL</b>		<b>UNCORRELATED RANDOM LATTICES</b>
		$\mu_P$	$\mu_{SC}$	$\mu_{AC}$
	<b>LATTICE FOURIER TRANSFORM</b>			
<b>ENERGY SPECTRUM</b>	$\mu_{AC}$	<b>PERIODIC CRYSTALS</b>		
	$\mu_{SC}$		<b>FIBONACCI PRECIOUS MEANS FIBONACCI-CLASS</b>	<b>MIXED MEANS (<math>n \geq m</math>)</b>
	$\mu_P$		<b>QUASIPERIODIC CRYSTALS</b>	<b>PERIOD DOUBLING METALLIC MEANS <math>m = \ell(\ell+1)</math> MIXED MEANS (<math>n &lt; m</math>)</b>
		$\Pi_0$	$\Pi_I$	$\Pi_{II}$
	<b>LATTICE FOURIER TRANSFORM</b>			

FIG. 1: (Top panel) Classification of aperiodic systems attending to the spectral measures of their lattice Fourier transform (abscissas) and their Hamiltonian spectrum energy (ordinates). (Bottom panel) Zoom out of the top panel first column showing the splitting of the pure point Fourier spectral measure  $\mu_P$  in four separate classes labeled  $\Pi_0$ ,  $\Pi_I$ ,  $\Pi_{II}$  and  $\Pi_{III}$  (more details in the text).

properties (emerging from the main features of the energy spectrum and the nature of its eigenstates), it is convenient to introduce the spectral charts depicted in Fig. 1.[8–13] In the top panel chart we provide a graphical classification scheme of aperiodic systems based on the nature of their diffraction spectra (in abscissas) and their energy spectra (in ordinates), respectively. In this way, the old-fashioned classification scheme based on the periodic-amorphous dichotomy is replaced by a much richer one, including nine different entries. In the upper left corner we have the periodic crystals exhibiting pure point Fourier spectra (discrete Bragg diffraction peaks) and an absolutely continuous energy spectrum (Bloch wave functions in allowed bands). In the lower right corner we have amorphous matter representatives, described in terms of uncorrelated random lattices, exhibiting an

absolutely continuous Fourier spectrum (diffuse spectra) and a pure point energy spectrum (exponentially localized wave functions).[14, 15] In the left lower corner we include the ideal quasicrystals, i.e., those without any sort of structural defect, since theoretical arguments suggest that in a perfect self-similar structure the presence of coherent resonance effects among the electronic states may efficiently induce their localization, leading to a perfectly insulating solid phase.[16, 17] In the right upper corner we locate Vogel spiral lattices, which provide an interesting instance of perfectly ordered systems where both translational and orientational symmetries are discarded. Accordingly, their Fourier transform does not show well-defined sharp spots, but diffuse rings similar to the electron diffraction patterns obtained from small areas of some amorphous materials.[11, 13] In the central row we include some one-dimensional aperiodic crystals which have been extensively studied in the literature during the last three decades, namely, Fibonacci, period doubling, Thue-Morse, and Rudin-Shapiro binary aperiodic crystals (BACs) based on the so-called substitution sequences. A substitution sequence is formally defined by the action of a substitution rule on an alphabet  $\mathcal{A} = \{A, B, C, \dots\}$ , consisting of a certain number of letters. The corresponding aperiodic sequence is then obtained by iterating the substitution rule starting from a given letter of the set  $\mathcal{A}$  in order to obtain an aperiodic string of letters, as it is shown in the second column of Table I for a two letters alphabet.

By inspecting the central row of Fig. 1 top panel, one realizes that although Fibonacci, Thue-Morse and Rudin-Shapiro BACs share the same kind of energy spectrum (a purely singular continuous one), they have different lattice Fourier transforms, so that these aperiodic crystals must be properly classified in separate categories. In turn, pure point lattice Fourier measures can be further split into four separate groups, namely, the so-called periodic ( $\Pi_0$ ), quasiperiodic ( $\Pi_I$ ), limit-quasiperiodic ( $\Pi_{II}$ ), and limit-periodic ( $\Pi_{III}$ ) pure point classes, respectively, by attending to finer details in their related diffraction patterns.[20, 22–25] The diffraction spectra of  $\Pi_0$  and  $\Pi_I$  classes representatives both consist in Bragg peaks supported by a *finite* Fourier module whose rank either equals the physical space dimension ( $\Pi_0$  class) or is larger than it ( $\Pi_I$  class). In the limit-quasiperiodic and limit-periodic classes  $\Pi_{II}$  and  $\Pi_{III}$  one also finds a diffraction spectrum consisting of a dense distribution of Bragg peaks. However, this distribution is supported by a Fourier module with a countably *infinity* of generators over the integers (i.e., the reciprocal space has infinite dimensions).[20, 26] The point-group symmetry of the diffraction spectrum of the limit-periodic structures belonging

to the  $\Pi_{\text{III}}$  spectral class is compatible with periodicity (unlike QCs) and their overall atomic structure can be described in terms of a union of periodic substructures with ever increasing lattice constants, forming a sequence of successive sublattices.[27, 28] Analogously, the diffraction spectrum of the limit-quasiperiodic class representatives can be generated by a superposition of spectra of an infinite number of quasiperiodic patterns. In fact, geometrically, a limit-quasiperiodic structure can be regarded as a section of a limit-periodic lattice in a higher dimension space, just as quasiperiodic structures can be obtained as sections of periodic lattices in high dimensions.[29] In the chart depicted in Fig. 1 bottom panel we properly zoom out the left column of Fig. 1 top panel spectral chart to provide some illustrative examples of several BACs exhibiting pure point spectra arranged according to the above scheme. Their corresponding spectral classes are also indicated in the last column of Table I.

To each substitution rule based on a binary alphabet we can associate a  $2 \times 2$  substitution matrix given by[30]

$$\mathbf{S} = \begin{pmatrix} n_A[g(A)] & n_A[g(B)] \\ n_B[g(A)] & n_B[g(B)] \end{pmatrix}, \quad (1)$$

where  $n_i[g(j)]$  indicates the number of times a given letter  $i$  appears in the substitution rule  $g(j)$ , irrespective of the order in which these letters occur. Accordingly, the substitution matrix does not give a complete description of a substitution rule, because different substitution rules can have the same substitution matrix (e.g. Thue-Morse and binary periodic sequences, see Table I). Notwithstanding this, one can obtain relevant information about the diffraction properties of different BACs by considering two algebraic properties of the corresponding substitution matrix, namely, their characteristic eigenvalues and their determinant value, which will allow to properly distinguish among the different pure point spectral classes.[31–33] Thus, if the substitution matrix characteristic polynomial contains a Pisot-Vijayaraghavan number,[34] and  $|\det \mathbf{S}| = 1$ , then the lattice belongs to the quasiperiodic class  $\Pi_{\text{I}}$ . Alternatively, if the sequence satisfies the Pisot property but  $|\det \mathbf{S}| \neq 1$ , then the lattice belongs to the limit-quasiperiodic  $\Pi_{\text{II}}$  class instead.[24, 25] Finally, if the sequence does not satisfy the Pisot property (i.e.,  $|\mu_-| \geq 1$ ) the lattice belongs to the limit-periodic  $\Pi_{\text{III}}$  class. Accordingly, the Pisot property  $\mu_+ > 1$  and  $|\mu_-| < 1$  provides a first criterion which demarcates certain aperiodic crystals possessing Bragg peaks from the rest. The unimodular condition  $|\det \mathbf{S}| = 1$  gives a second criterion to distinguish between QCs

( $\Pi_I$  class) and limit-quasiperiodic structures ( $\Pi_{II}$  class).[35]

In this work we perform an analytical study of the zeroth-order energy spectrum of *general* BACs characterized by the presence of *both* atomic and chemical bonding aperiodic distributions described by means of mixed-type Hamiltonians which include both diagonal and off-diagonal terms aperiodically distributed. To this end, in Sec. II we will introduce an algebraic approach which efficiently exploits the hierarchical structure of BACs based on substitution sequences in order to properly disclose their related self-similar structure. This approach allows us to properly highlight chemical correlation effects present in the underlying lattice of general BACs in terms of suitable blocking schemes including two elemental *block* matrices for each considered BAC. In so doing, we obtain a renormalized sequence of local transfer matrices describing an effective binary alloy which preserves the original BAC atomic order. In Sec. III we calculate the commutators related to these elemental block matrices sets to derive the zeroth-order structure of the electronic energy spectra of several representatives of the  $\Pi_I$ ,  $\Pi_{II}$ , and  $\Pi_{III}$  spectral classes, all of them exhibiting singular continuous energy spectra along with pure point diffraction spectra. In this way, we realize that all the considered commutators share a common mathematical structure consisting of an energy dependent polynomial multiplying a null trace matrix. By inspecting the degree of these polynomial factors we confirm that there exists a direct correlation between the polynomial degree and the structural complexity of the considered BAC. We also disclose the existence of a resonance energy which defines the basic anatomy of the zeroth-order energy spectra structure for the standard Fibonacci, the precious means and the Fibonacci-class QCs. This eigenstate can also be found in the energy spectra of BACs belonging to the spectral classes  $\Pi_{II}$  and  $\Pi_{III}$ , although for specific particular choices of the corresponding model parameters only. The nature of these resonant eigenstates and their role in the resulting transport properties is studied in Sec.IV by deriving close analytical expressions for their transmission coefficients, which are directly related to the Landauer conductance of the considered BACs connected to two metallic leads. Finally, the main results obtained in this study and their physical implications are discussed in the concluding Sec.V.

## GENERAL BINARY APERIODIC CRYSTALS: A UNIFIED TREATMENT

In this work we will consider one-dimensional binary crystals where two kinds of atoms, say  $A$  and  $B$ , are arranged aperiodically according to certain substitution sequences listed in Table I. Within the electron independent approximation the electron dynamics through these alloys can be described in terms of a tight-binding model given by the Schrödinger equation (in  $\hbar = 2m = 1$  units)

$$(E - V_k)\psi_k - t_{k,k-1}\psi_{k-1} - t_{k,k+1}\psi_{k+1} = 0, \quad (2)$$

where  $E$  is the electron energy, the on-site energies  $V_k$  account for the atomic potentials at the  $k$ -th lattice site, the transfer integrals  $t_{k,k\pm 1}$  measure the hopping amplitudes of the electron between neighboring atoms, and  $\psi_k$  stands for the amplitude of the wave function at site  $k$ . Since the properties of a chemical bond linking two different atoms generally depend on their chemical nature, we will explicitly consider that the aperiodic sequence of atoms along the chain naturally induces an aperiodic sequence of bonds in the considered alloy. Accordingly, *general* BACs are characterized by the presence of *both* atomic and chemical bonding aperiodic distributions. This feature properly distinguishes the BACs studied in this work from both the purely geometric on-site (i.e.,  $t_{k,k\pm 1} \equiv 1, \forall k$ ) and the chemically unrealistic transfer (i.e.,  $V_k \equiv 0, \forall k$ ) models, which have been widely considered in the physical and mathematical literature during the last three decades.[4, 10, 36–38]

After Eq.(2) the wave function amplitudes can be recursively obtained from the matrix expression

$$\begin{pmatrix} \psi_{N+1} \\ \psi_N \end{pmatrix} = \prod_{k=N}^1 \mathbf{T}_{k,k\pm 1} \begin{pmatrix} \psi_1 \\ \psi_0 \end{pmatrix} \equiv \mathcal{M}_N(E) \begin{pmatrix} \psi_1 \\ \psi_0 \end{pmatrix}, \quad (3)$$

where

$$\mathbf{T}_{k,k\pm 1} = \begin{pmatrix} \frac{E-V_k}{t_{k,k+1}} - \frac{t_{k,k-1}}{t_{k,k+1}} & \\ 1 & 0 \end{pmatrix}, \quad (4)$$

is referred to as the local transfer matrix, and  $\mathcal{M}_N(E)$  is the so-called global transfer matrix. Since the arrangement of transfer integrals  $t_{AA}$ ,  $t_{AB} = t_{BA}$  and  $t_{BB}$  is synchronized with the atomic on-site energies sequence  $\{V_k\}$ , the underlying aperiodic order of the atoms and bonds in general BACs is naturally expressed by: (1) the number of different *kinds* of local transfer matrices which must be considered in the  $\mathcal{M}_N$  product, and (2) the specific *order* of appearance of these local transfer matrices in  $\mathcal{M}_N(E)$ .

## Local transfer matrices classification

According to Eq.(4) any given local transfer matrix is completely determined by a triplet formed by three consecutive atoms along the lattice. The role played by each atom of the triplet can be disclosed making use of the decomposition property,[39, 40]

$$\mathbf{T}_{k,k\pm 1} = \begin{pmatrix} t_{k,k+1}^{-1} & 0 \\ 0 & 1 \end{pmatrix} \begin{pmatrix} \alpha_k & -1 \\ 1 & 0 \end{pmatrix} \begin{pmatrix} 1 & 0 \\ 0 & t_{k,k-1} \end{pmatrix} \equiv \mathbf{G}_R \mathbf{A}_k \mathbf{G}_L, \quad (5)$$

where  $\alpha_k \equiv E - V_k$ ,  $\mathbf{A}_k$  describes the central atom energy contribution, and the matrices  $\mathbf{G}_R$  ( $\mathbf{G}_L$ ) describe its right (left) bond strength with the neighboring atoms, respectively. We note that  $\mathbf{A}_k$  belongs to the  $SL(2, \mathbb{R})$  group (i.e.,  $\det \mathbf{A}_k = 1$ ), whereas the bond matrices generally do not. By inspecting Eq.(5) we readily see that there exist eight possible local transfer matrices in a general BAC. Four of them are related to triplets containing a central  $A$  type atom, namely

$$\mathbf{T}_{BAB} = \begin{pmatrix} \alpha_A & -1 \\ 1 & 0 \end{pmatrix}, \quad \mathbf{T}_{AAB} = \begin{pmatrix} \alpha_A & -\gamma_A \\ 1 & 0 \end{pmatrix}, \quad \mathbf{T}_{BAA} = \begin{pmatrix} \frac{\alpha_A}{\gamma_A} & -\frac{1}{\gamma_A} \\ 1 & 0 \end{pmatrix}, \quad \mathbf{T}_{AAA} = \begin{pmatrix} \frac{\alpha_A}{\gamma_A} & -1 \\ 1 & 0 \end{pmatrix}, \quad (6)$$

where we have adopted the energy scale  $t_{AB} \equiv 1$  and  $\gamma_A \equiv t_{AA}$  without loss of generality. Note that the local transfer matrices corresponding to both the  $AAA$  triplet and the isolated  $A$  atom belong to the  $SL(2, \mathbb{R})$  group due to the mirror symmetry of the bonds with respect to the center atom. The other four local transfer matrices are related to triplets containing a central  $B$  type atom, and they can be straightforwardly obtained from the previous ones by performing the conjugation operation  $A \leftrightarrow B$  to obtain

$$\mathbf{T}_{ABA} = \begin{pmatrix} \alpha_B & -1 \\ 1 & 0 \end{pmatrix}, \quad \mathbf{T}_{BBA} = \begin{pmatrix} \alpha_B & -\gamma_B \\ 1 & 0 \end{pmatrix}, \quad \mathbf{T}_{ABB} = \begin{pmatrix} \frac{\alpha_B}{\gamma_B} & -\frac{1}{\gamma_B} \\ 1 & 0 \end{pmatrix}, \quad \mathbf{T}_{BBB} = \begin{pmatrix} \frac{\alpha_B}{\gamma_B} & -1 \\ 1 & 0 \end{pmatrix}, \quad (7)$$

where  $\gamma_B \equiv t_{BB}$ .

Within this framework, a measure of the structural *complexity degree* of a given BAC can be estimated by counting the number of different kinds of local transfer matrices which are necessary to fully describe its topological order. For the sake of illustration in Fig. 2 we pictorially classify several BACs attending to the number of different local transfer matrices required to this end. Let us recall that the so-called complexity function  $P(k, w)$



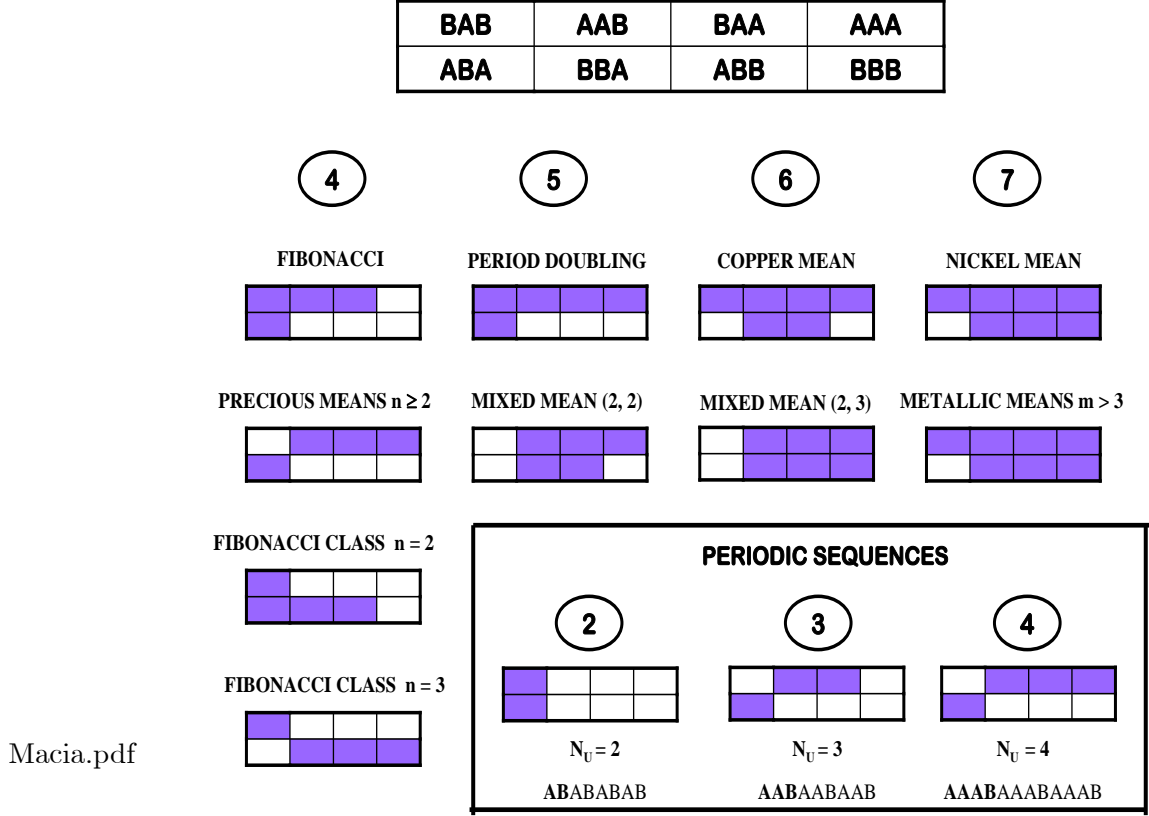


FIG. 2: Classification of periodic (bottom right panel, where  $N_U$  indicates the unit cell size) and BACs according to the number (encircled) of different local matrices (shadowed boxes) required to fully describe their topological order at the triplet scale. The key for the local transfer matrices subscript labeling is given in the top panel.

measures the number of different words  $w_i$  of length  $k$  that appear in an infinite sequence of letters.[6] The minimal complexity sequences have  $P(k, w) = k$  (periodic) and  $P(k, w) = k + 1$  (Sturmian). Random sequences are characterized by  $P(k, w) = 2^k$ . Accordingly, the possible number of different local transfer matrices ( $k = 3$ ) is then bounded by the values 3 (periodic) and 8 (random). As we see, BACs based on the precious means and the Fibonacci-class families (both including the standard Fibonacci sequence as a particular case) require four different local transfer matrices. In this regard their local topological complexity is comparable to that of *periodic* lattices with a relatively large unit cell (e. g., *AAAB* or *AABB*, and their related cyclic permutations, see the bottom panel in Fig. 2). The BACs based on the period doubling and the mixed means sequences with  $n \geq m$ , both requiring

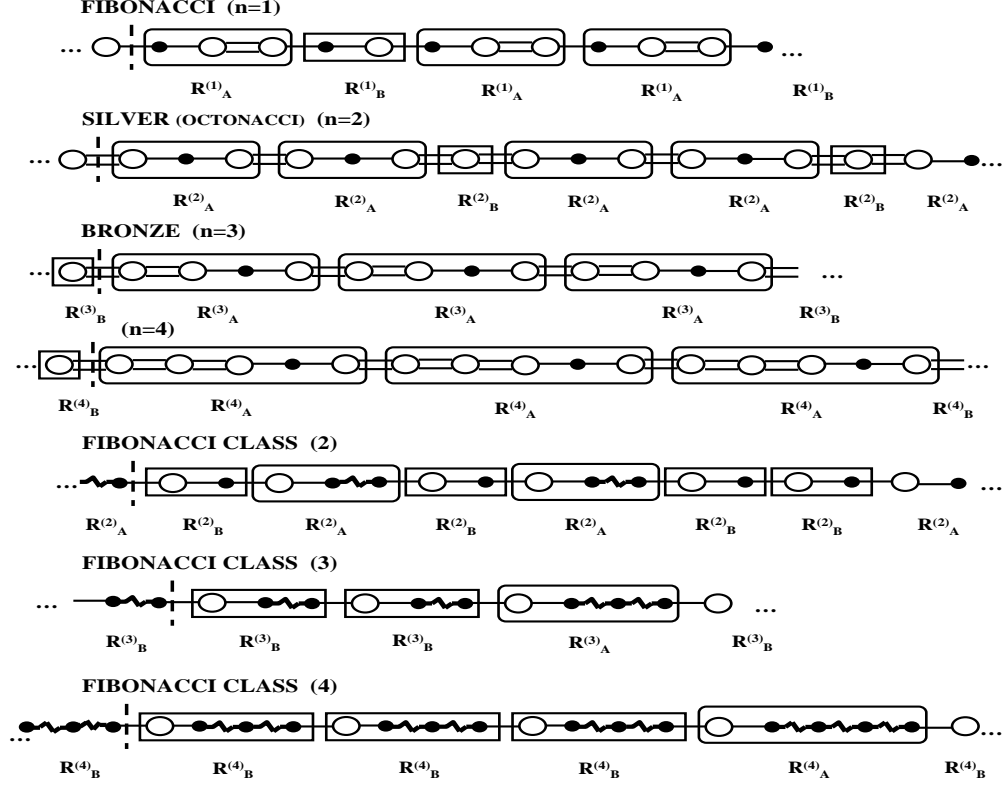
the knowledge of five different local transfer matrices, are examples of the next level of local complexity. The BACs based on the copper mean sequence (the first representative of the so-called metallic means family) and the mixed mean sequence with  $n < m$ , belong to the next complexity level, which requires the knowledge of six different local transfer matrices. Finally, BACs based on metallic mean substitution rules with  $m \geq 3$  need seven different  $\mathbf{T}_{k,k\pm 1}$  matrices, thereby exhibiting a remarkable degree of topological complexity at the triplet atomic scale. We note that none of the BACs based on the substitution rules listed in Table I exhibit the maximum possible complexity degree.[41]

### Self-similar blocking schemes

The next step towards a unified description of general BACs focuses on the particular order of appearance of the different local transfer matrices along the chain, ultimately determining the global transfer matrix  $\mathcal{M}_N(E)$ , as prescribed by Eq.(3). Our strategy will be to exploit the hierarchical structure of BACs based on substitution sequences in order to properly disclose their related long-range correlations. To this end, we will zoom out the considered spatial scale, going from the nearest-neighbors scale related to the triplet level description all the way up to the entire lattice size scale. To achieve this goal, we will rewrite the global transfer matrix  $\mathcal{M}_N(E)$  of *any* given BAC in terms of *just two block* matrices  $\mathbf{R}_A^{(n,m)}$  and  $\mathbf{R}_B^{(n,m)}$  in the form,[10, 42–44]

$$\mathcal{M}_N(E) = \prod_{k=N}^1 \mathbf{T}_{k,k\pm 1} \equiv \dots \mathbf{R}_B^{(n,m)} \mathbf{R}_A^{(n,m)} \mathbf{R}_A^{(n,m)} \mathbf{R}_B^{(n,m)} \mathbf{R}_A^{(n,m)} \quad (8)$$

according to certain *blocking schemes* which are shown in Figs.3-5 for BACs based on different substitution sequences. A close comparison of the lettering corresponding to the BACs depicted in Figs. 3-5 with the information provided in Table II clearly indicates that the topological order present in the original *atomic* lattice is preserved by the block matrices sequence appearing in Eq.(8). Thus, albeit the number of  $\mathbf{T}_{k,k\pm 1}$  matrices we must consider at the triplet scale level can vary from four to eight in general BACs, the recourse to appropriate block matrices sets allows one to express the global  $\mathcal{M}_N(E)$  matrix in a considerably simplified way, corresponding to an effective binary alloy which preserves the original BAC atomic order. In other words, the topological order of the sequence of atoms  $\{V_k\}$  is naturally translated to the block matrices sequence, which obeys the same substitution rule.



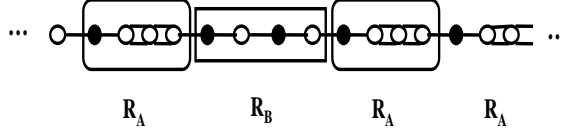
Macia.pdf

FIG. 3: Elemental block matrices schemes for BACs based on substitution sequences belonging to the quasiperiodic  $\Pi_I$  class. From top to bottom we display the first representatives of the precious means and Fibonacci-class families, respectively. White (black) circles denote  $A$  ( $B$ ) type atoms and  $t_{AB}$ ,  $t_{AA}$ , and  $t_{BB}$  transfer integrals are represented by single bonds, double bonds and zigzag bonds, respectively. In order to complete the blocking schemes the atoms at both ends are connected to each other by adopting cyclic boundary conditions. The vertical dashed line indicates the reading frame origin (from left to right). We note that the elemental block matrices appear in reversed order in the global matrix given by Eq.(8).

This characteristic feature of the block matrices is shown in Table II for the BACs based on the substitution sequences listed in Table I. Accordingly, the matrices  $\mathbf{R}_{A,B}^{(n,m)}$  will be referred to as *elemental* block matrices thereafter.

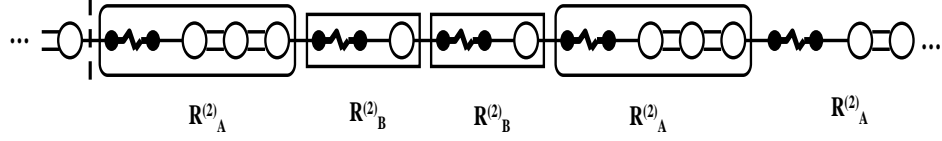
We note that the block matrices  $\mathbf{R}_A^{(n,m)}$  and  $\mathbf{R}_B^{(n,m)}$  present in Eq.(8) cannot be properly regarded as local transfer matrices themselves, since they lack the required form prescribed by Eq.(4). This is not surprising at all, since block matrices no longer relate the physical

### PERIOD DOUBLING

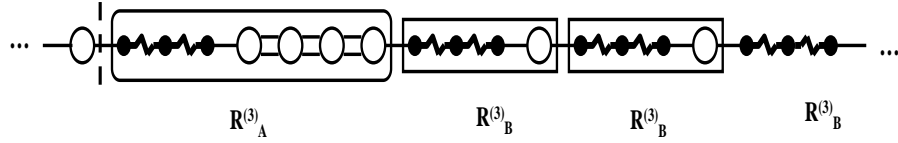


### METALLIC MEANS

#### COPPER (m=2)



#### NICKEL (m=3)



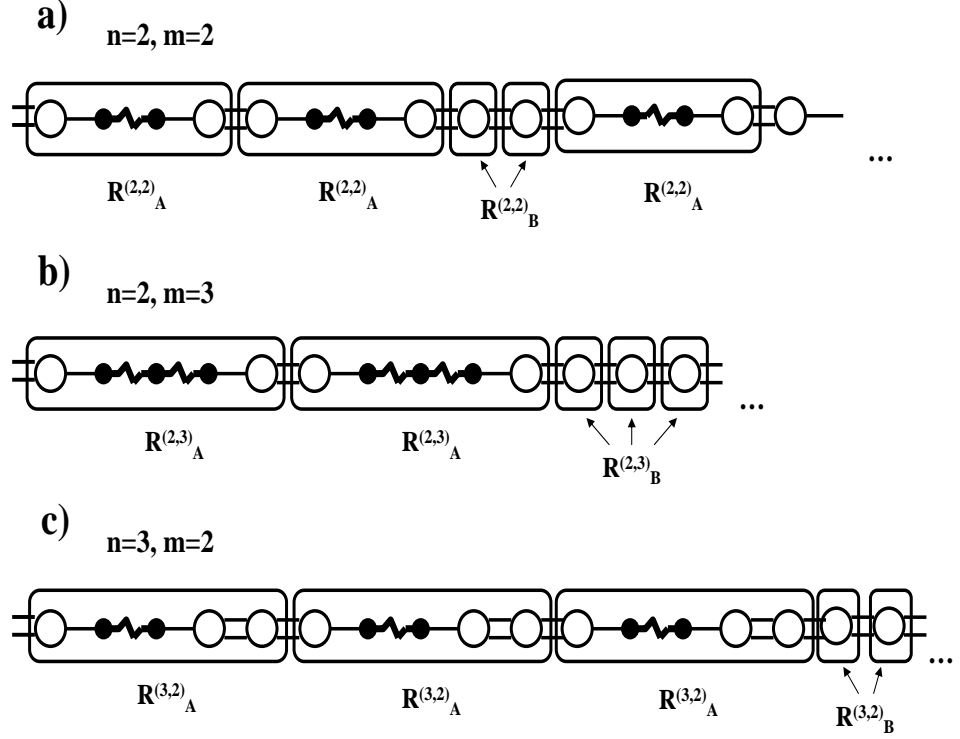
Macia.pdf

FIG. 4: Elemental block matrices schemes for BACs based on the period doubling sequence and the two first representatives of the metallic mean sequences, all of them belonging to the limit-periodic  $\Pi_{III}$  class. The adopted notation is the same as in Fig. 3.

properties of three consecutive atomic sites, but they describe the dynamics of electrons extending over longer spatial scales, so that these matrices become specially well suited to deal with transport features stemming from the long-range order in BACs. In fact, by properly scaling the original chain in terms of successively longer block matrices, one is able to fully exploit the inflation/deflation symmetry characteristic of *any* BAC generated from a substitution rule in order to describe the electronic state at sites more and more farther apart.

The total number of local transfer matrices in  $\mathcal{M}_N(E)$  is naturally reduced due to the blocking process. In fact, by inspecting Figs.3-5 we see that the number of block matrices decreases by two generation orders as compared to the number of atoms present in the original lattice. For instance, if  $N = F_j$  is the number of atomic lattice sites in the standard

# MIXED MEANS



Macia.pdf

FIG. 5: Elemental block matrices schemes for BACs based on the lowest order mixed means representatives, belonging to either the limit-quasiperiodic  $\Pi_{II}$  ( $n \geq m$ ) or the limit-periodic  $\Pi_{III}$  ( $n < m$ ) classes, respectively. The adopted notation is the same as in Fig. 3.

Fibonacci chain, one can show by induction that the block matrices sequence contains  $n_A = F_{j-3}$  matrices  $\mathbf{R}_A^{(1)}$  and  $n_B = F_{j-4}$  matrices  $\mathbf{R}_B^{(1)}$ , where  $F_j = F_{j-1} + F_{j-2}$ , with  $F_0 = F_1 = 1$ , are the so-called Fibonacci numbers. Similar results can be readily obtained for the other considered BACs. Accordingly, the choice of appropriate elemental block matrices obeying certain self-similar schemes can be regarded as an effective *renormalization* of the original local transfer matrices sequence.[10, 42]

In fact, from a physical point of view these matrices respectively describe the electron dynamics through the minimal atomic clusters in terms of which the entire BAC can be decomposed via an exact deflation process. For instance, in the case of a Fibonacci QC these atomic clusters are  $BA$  and  $BAA$ . In this regard, it is worth noticing that a decomposition scheme based on the mirror reversed  $AB$  and  $AAB$  atomic clusters has been recently

considered, in order to study the dynamics of classical particles in a time-driven Fibonacci lattice.[45] Alternatively, one may consider non-minimal blocking schemes allowing for an exact decomposition of the  $M_N$  matrix string in terms of longer atomic clusters, in such a way that the resulting blocking schemes also preserve the characteristic aperiodic order of the structure. For instance, by introducing the block matrices  $\tilde{R}_A^{(1)} \equiv R_B^{(1)} R_A^{(1)} R_A^{(1)}$  and  $\tilde{R}_B^{(1)} \equiv R_B^{(1)} R_A^{(1)}$ , one can readily check that any  $n$  stage  $M_N$  matrix, renormalized in terms of  $R_A^{(1)}$  and  $R_B^{(1)}$  elemental blocks, is mapped into a  $n - 2$  stage one in terms of  $\tilde{R}_A^{(1)}$  and  $\tilde{R}_B^{(1)}$  blocks in a Fibonacci QC.

By inspecting Table II several conclusions can be drawn: (1) the Fibonacci lattice elemental block matrices  $\mathbf{R}_A^{(1)}$  and  $\mathbf{R}_B^{(1)}$  are related to those corresponding to the Fibonacci-class ( $n = 2$ ) ones,  $\mathbf{R}_A^{(2)}$  and  $\mathbf{R}_B^{(2)}$ , by the conjugation operation  $A \leftrightarrow B$ , (2) all of the BACs belonging to the precious mean family with  $n > 1$  share the same type of  $\mathbf{R}_B^{(n)}$  elemental block matrix (describing AAA triplets) whereas the  $\mathbf{R}_A^{(n)}$  block matrices are related to atomic strings of the form  $A^{n-1}BA$  (see Fig.3), (3) the elemental block matrices for Fibonacci-class based QCs corresponding to consecutive generator sequence numbers,  $n - 1$  and  $n$ , are related through the relationship  $\mathbf{R}_B^{(n)} = \mathbf{R}_A^{(n-1)}$ . For a given  $n$  value the  $\mathbf{R}_A^{(n)}$  block matrices are systematically related to atomic strings of the form  $AB^n$  along the chain (see Fig.3), (4) in a similar way, the block matrices for BACs based on the metallic means substitution sequence are systematically related to atomic strings of the form  $B^m A^{m+1}$  for  $\mathbf{R}_A^{(m)}$  matrices and  $B^m A$  for  $\mathbf{R}_B^{(m)}$  matrices (see Fig.4), and (5) all of the BACs based on mixed means substitution sequences have the same type of  $\mathbf{R}_B^{(n,m)}$  block matrix (describing AAA triplets as in the case of precious means based BACs), whereas the form of the  $\mathbf{R}_A^{(n,m)}$  block matrix depends on the  $n$  and  $m$  values: it is completely analogous to that corresponding to precious mean based BACs (i.e.,  $\mathbf{R}_A^{(n,m)} = \mathbf{R}_A^{(n-1,m)} \mathbf{T}_{AAA}$ ) when  $n \geq m$ , while a  $\mathbf{T}_{BBB}$  local transfer matrix is inserted in the middle of the  $\mathbf{R}_A^{(n-1,m)}$  matrix in the case  $n < m$ .

## ZERO-ORDER ENERGY SPECTRA

### Fibonacci quasicrystals

For the sake of illustration, let us first consider the electronic structure of QCs based on the standard Fibonacci substitution rule  $g(A) = AB$  and  $g(B) = A$ . Making use of Eqs.(6)

and (7), and according to Table II, the corresponding elemental block matrices are given by

$$\mathbf{R}_A^{(1)} = \gamma_A^{-1} \begin{pmatrix} R_{11}(E) & \gamma_A^2 - (E - \epsilon)^2 \\ E^2 - \epsilon^2 - 1 & \epsilon - E \end{pmatrix}, \quad \mathbf{R}_B^{(1)} = \begin{pmatrix} E^2 - \epsilon^2 - 1 & \epsilon - E \\ \epsilon + E & -1 \end{pmatrix}, \quad (9)$$

with  $R_{11}(E) = (E + \epsilon)[(E - \epsilon)^2 - \gamma_A^2] + \epsilon - E$ , where without loss of generality the origin of energies is defined in such a way that  $V_A = \epsilon = -V_B$ , so that  $\alpha_A = E - \epsilon$ , and  $\alpha_B = E + \epsilon$ , henceforth. As we see, the matrix elements of both elemental block matrices are polynomials of the electron energy, so that one may look for the possible existence of resonance energies satisfying the condition  $[\mathbf{R}_A^{(1)}, \mathbf{R}_B^{(1)}] = \mathbf{0}$ . By explicitly evaluating the commutator we get

$$[\mathbf{R}_A^{(1)}, \mathbf{R}_B^{(1)}] = \gamma_A^{-1} \Lambda_A(E, \epsilon, \gamma_A) \begin{pmatrix} 1 & 0 \\ E + \epsilon & -1 \end{pmatrix} \equiv \gamma_A^{-1} \Lambda_A \mathbf{F}_1, \quad (10)$$

where we have introduced the polynomial  $\Lambda_A(E, \epsilon, \gamma_A) \equiv \epsilon(1 + \gamma_A^2) - E(1 - \gamma_A^2)$ . Therefore, for any realization of the general binary Fibonacci alloy (i. e. for any combination of  $\epsilon$  and  $\gamma_A \neq 1$  values) there *always* exists one energy satisfying the relation  $\Lambda_A(E, \epsilon, \gamma_A) = 0$ , namely,[42, 47]

$$E_* = \epsilon \frac{1 + \gamma_A^2}{1 - \gamma_A^2}, \quad (11)$$

which defines the zeroth-order energy spectrum structure. For this energy value the global transfer matrix of the system can be explicitly evaluated in the closed form[42]

$$\mathcal{M}_N^{(1)}(E_*) \equiv [\mathbf{R}_A^{(1)}]^{n_A} [\mathbf{R}_B^{(1)}]^{n_B} = \begin{pmatrix} U_N & -\gamma_A U_{N-1} \\ \gamma_A^{-1} U_{N-1} & -U_{N-2} \end{pmatrix}, \quad (12)$$

where  $U_k(x)$ , with  $x \equiv \sqrt{E_*^2 - \epsilon^2}/2 \equiv \cos \phi$ , are Chebyshev polynomials of the second kind. Taking into account the relationship  $U_k - U_{k-2} = 2T_k$  between Chebyshev polynomials of the first and second kinds, from Eq.(12) we get  $\text{tr}[\mathcal{M}_N^{(1)}(E_*)] = 2 \cos(N\phi) \leq 2$ . Consequently, we can ensure that the bi-parametric set of energies  $E_*(\epsilon, \gamma_A)$  belongs to the spectrum in the quasiperiodic limit  $N \rightarrow \infty$ . An illustrative example of the energy spectra of general Fibonacci QCs for different values of the model parameter  $\gamma_A$  is shown in Fig.6. One can appreciate that the resonant states given by Eq.(11) are located across the densest region of the phase diagram.

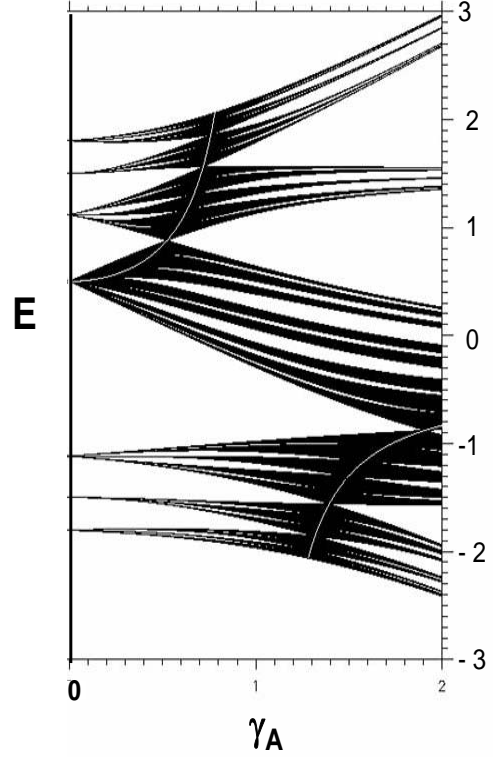


FIG. 6: Numerically obtained phase diagram for a binary Fibonacci QC with  $N = 34$  atoms and on-site energy  $\epsilon = 1/2$ , over the range  $0 \leq \gamma_A \leq 2$ . The zeroth-order energy spectrum given by Eq.(11) is highlighted with a thin white line. The regions closer to this line are densely populated as a consequence of the high degeneration of the resonance energy  $E_*$ . We note that  $E_*(\gamma^{-1}) = -E_*(\gamma)$ .

### Precious means quasicrystals

The so-called precious means based QCs are obtained from the substitution rule  $g(A) = A^n B$ ,  $g(B) = A$  with  $n \geq 2$  (see Table I). Among the first members of this family we find the silver mean ( $n = 2$ ) and the bronze mean ( $n = 3$ ). In these sequences  $B$  atoms always appear isolated, while  $A$  atoms form clusters including  $n$  or  $n + 1$  atoms each (see Fig.3). Their substitution matrix eigenvalues read  $\mu_{\pm} = (n \pm \sqrt{n^2 + 4})/2$ . Since  $\sqrt{n^2 + 4} > n$  we conclude that all the representatives of this family satisfy the Pisot property. In addition, we have  $|\det \mathbf{S}| = 1 \ \forall n$ , so that the corresponding BACs belong to the  $\Pi_I$  quasiperiodic class.

Making use of the elemental block matrices definitions listed in Table II for the silver



mean based QC we obtain  $[\mathbf{R}_A^{(2)}, \mathbf{R}_B^{(2)}] = -\gamma_A^{-1} \Lambda_A \mathbf{F}_2$ , where  $\mathbf{F}_2 = \sigma_x$  is a Pauli matrix. Similarly, making use of the elemental block matrices definitions listed in Table II for the bronze mean based QC we obtain  $[\mathbf{R}_A^{(3)}, \mathbf{R}_B^{(3)}] = -\gamma_A^{-1} \Lambda_A \mathbf{F}_3$ , where  $\mathbf{F}_3 \equiv \sigma_x \mathbf{T}_{AAA}$ . As we see, both commutators have the same algebraic structure as that corresponding to the standard Fibonacci QC, namely, the energy dependent polynomial factor  $\Lambda_A$  multiplying a null trace matrix. In fact, this is a common feature shared by all of the commutators related to the precious mean based QCs. To show this we will exploit the relationships  $\mathbf{R}_A^{(n)} = \mathbf{R}_A^{(n-1)} \mathbf{T}_{AAA}$  and  $\mathbf{R}_B^{(n)} = \mathbf{T}_{AAA} \mathbf{R}_A^{(n-1)}$   $\forall n > 2$ , listed in Table II, in order to express the commutator corresponding to the general case in the form

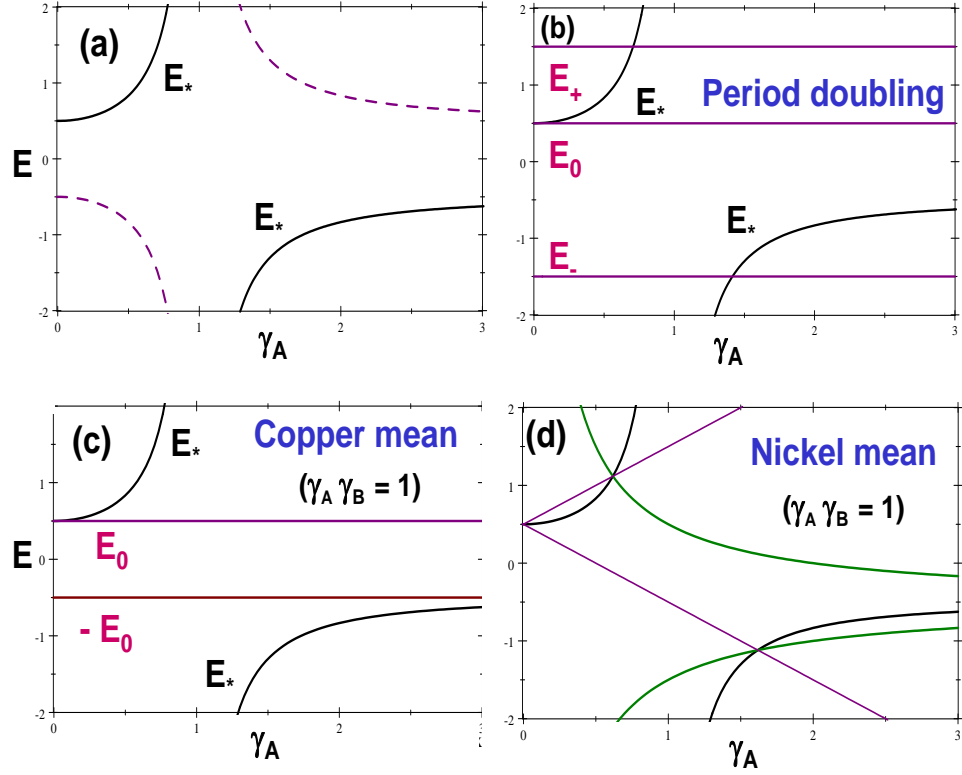
$$\begin{aligned} [\mathbf{R}_A^{(n)}, \mathbf{R}_B^{(n)}] &= [\mathbf{R}_A^{(n-1)} \mathbf{T}_{AAA}, \mathbf{T}_{AAA} \mathbf{R}_A^{(n-1)}] \equiv \mathbf{R}_A^{(n-1)} \mathbf{T}_{AAA} \mathbf{T}_{AAA} - \mathbf{T}_{AAA} \mathbf{R}_A^{(n-1)} \mathbf{T}_{AAA} \\ &= \mathbf{R}_A^{(n-1)} \mathbf{R}_B^{(n-1)} \mathbf{T}_{AAA} - \mathbf{R}_B^{(n-1)} \mathbf{R}_A^{(n-1)} \mathbf{T}_{AAA} = [\mathbf{R}_A^{(n-1)}, \mathbf{R}_B^{(n-1)}] \mathbf{T}_{AAA}. \end{aligned} \quad (13)$$

Then, iterating Eq.(13) backwards we obtain

$$[\mathbf{R}_A^{(n)}, \mathbf{R}_B^{(n)}] = [\mathbf{R}_A^{(2)}, \mathbf{R}_B^{(2)}] \mathbf{T}_{AAA}^{n-2} = -\gamma_A^{-1} \Lambda_A \sigma_x \mathbf{T}_{AAA}^{n-2}, \quad n \geq 2. \quad (14)$$

Accordingly, the fundamental structure of commutators corresponding to QCs based on the precious means sequences can be expressed as a product involving the polynomial factor  $\Lambda_A$ , the Pauli matrix  $\sigma_x$ , and a power of the local transfer matrix  $\mathbf{T}_{AAA}$ , which is naturally related to the existence of longer and longer strings of  $A$  type atoms in the corresponding QCs when  $n$  is progressively increased (see Fig. 3). Thus, the energy dependent polynomial  $\Lambda_A(E, \epsilon, \gamma)$ , originally appearing in the commutator of the standard Fibonacci QC, is inherited by all the precious mean QCs commutators in a natural way.

In order to analyze the solutions to the general resonance condition  $[\mathbf{R}_A^{(n)}, \mathbf{R}_B^{(n)}] = \mathbf{0}$ , it is convenient to recall that the necessary condition for the equation  $\mathbf{A}\mathbf{B} = \mathbf{0}$  to be satisfied by two arbitrary square matrices ( $\mathbf{A} \neq \mathbf{0}$  and  $\mathbf{B} \neq \mathbf{0}$ ) is that one of the matrices appearing in the product has zero determinant. Then, since  $\det \sigma_x = -1$  and  $\det(\mathbf{T}_{AAA}^{n-2}) = 1 \quad \forall n$  ( $\mathbf{T}_{AAA} \in SL(2, \mathbb{R})$ ), we conclude that  $\sigma_x \mathbf{T}_{AAA}^{n-2} \neq \mathbf{0} \quad \forall n \geq 2$ . Consequently, the commutation condition  $[\mathbf{R}_A^{(n)}, \mathbf{R}_B^{(n)}] = \mathbf{0}$ , reduces to the algebraic equation  $\Lambda_A(E) = 0 \quad \forall n$ , leading to the *same* resonance energy  $E_*$  that was obtained in the study of the Fibonacci QC. This is a very remarkable result, for it indicates that the zeroth-order structure of the electronic energy spectra of all precious means based QCs relies on a common resonance energy state at their very fundamental level. Therefore, the set of states highlighted by the thin white



Macia2.pdf

FIG. 7: Phase diagrams showing the analytical zeroth-order spectra of (a) general precious mean (solid line) and Fibonacci-class  $FC(n)$  (dashed line)  $\Pi_I$  class QCs, and the  $\Pi_{III}$  class, (b) general period doubling ( $E_0 = 1/2$ ,  $E_{\pm} = \pm 3/2$ ), (c) copper mean ( $E_0 = 1/2$ ) and (d) nickel mean limit-periodic crystals for the particular case  $\gamma_B = \gamma_A^{-1}$  (more details in the text).

lines in the standard Fibonacci phase diagram shown in Fig. 6, will also be present in *every* energy spectrum of *any* QC based on a precious mean sequence, as is illustrated in Fig.7(a).

### Fibonacci-class quasicrystals

It is natural to wonder as to whether the results obtained in the preceeding section also hold for the so-called Fibonacci-class lattices  $FC(n)$ , obtained from the application of the substitution rule  $g(A) = B^{n-1}AB$ ,  $g(B) = B^{n-1}A$  (see Table I), which trivially reduces to the standard Fibonacci QC in the case  $n = 1$ . Indeed, this substitution sequence was originally introduced in order to generalize the standard Fibonacci lattices,[48] and we note that

by defining  $A' \equiv B^{n-1}A$  the proposed substitution rule reduces to the standard Fibonacci one for  $n \neq 1$  as well. By inspecting Table I one realizes that the  $\text{FC}(n)$  related substitution matrices share the same characteristic polynomial as the previous means related ones, and can thus be considered as formally equivalent as regarding the Pisot and unimodularity properties. Thus, the  $\text{FC}(n)$  based QCs also belong to the quasiperiodic  $\Pi_I$  class.

Making use of the elemental block matrices definitions listed in Table II for the first representative,  $\text{FC}(2)$ , we obtain

$$\left[ \mathbf{R}_A^{(2)}, \mathbf{R}_B^{(2)} \right]^{\text{FC}} = \gamma_B^{-1} \Lambda_B(E, \epsilon, \gamma_B) \begin{pmatrix} 1 & 0 \\ E - \epsilon & -1 \end{pmatrix} \equiv \gamma_B^{-1} \Lambda_B(E, \epsilon, \gamma_B) \tilde{\mathbf{F}}_1, \quad (15)$$

where  $\Lambda_B(E, \epsilon, \gamma_B) \equiv -\epsilon(1 + \gamma_B^2) - E(1 - \gamma_B^2)$ , and the superscript FC is introduced to distinguish this commutator from that corresponding to the silver mean lattice. By comparing with Eq.(10) we realize that the  $\text{FC}(2)$  commutator can be obtained from the standard Fibonacci one upon the conjugation operation  $\epsilon \rightarrow -\epsilon$  and  $\gamma_A \rightarrow \gamma_B$ , so that we have the formal relationship

$$\left[ \mathbf{R}_A^{(2)}, \mathbf{R}_B^{(2)} \right]^{\text{FC}} = \mathcal{C} \cdot \left[ \mathbf{R}_A^{(1)}, \mathbf{R}_B^{(1)} \right] \equiv \gamma_B^{-1} \Lambda_B(E, \epsilon, \gamma_B) \mathcal{C} \cdot \mathbf{F}_1, \quad (16)$$

with  $\Lambda_B(E, \epsilon, \gamma_B) = \mathcal{C} \cdot \Lambda_A(E, \epsilon, \gamma_A)$ , where  $\mathcal{C} \cdot$  denotes the conjugation operation. Thus, the resonance condition for any  $\text{FC}(n)$  QC realization (i. e., for any combination of  $\epsilon$  and  $\gamma_B \neq 1$  values) is given by the energy values satisfying the relation  $\Lambda_B(E, \epsilon, \gamma_B) = 0$ , namely,

$$E_*^{\text{FC}} = -\epsilon \frac{1 + \gamma_B^2}{1 - \gamma_B^2} = \mathcal{C} \cdot E_*, \quad (17)$$

where  $E_*$  is the standard Fibonacci resonance energy given by Eq.(11).

Quite interestingly, the general relation  $\left[ \mathbf{R}_A^{(n)}, \mathbf{R}_B^{(n)} \right]^{\text{FC}} = \gamma_B^{-1} \Lambda_B(E, \epsilon, \gamma_B) \tilde{\mathbf{F}}_1$ ,  $\forall n \geq 2$ , can be proved as follows. According to the relationship  $\mathbf{R}_B^{(n)} = \mathbf{R}_A^{(n-1)}$  (see Table II) we can express  $\left[ \mathbf{R}_A^{(n)}, \mathbf{R}_B^{(n)} \right]^{\text{FC}} = \left[ \mathbf{R}_A^{(n)}, \mathbf{R}_A^{(n-1)} \right]^{\text{FC}} = \left[ \mathbf{R}_A^{(3)}, \mathbf{R}_A^{(2)} \right]^{\text{FC}}$ , where we have iterated backwards. By properly inserting the identity matrix  $\mathbf{T}_{BBA}^{-1} \mathbf{T}_{BBA}$  on the right of the  $\mathbf{T}_{BBB}$  matrix appearing in  $\mathbf{R}_A^{(3)}$  (see Table II) we get  $\mathbf{R}_A^{(3)} = \mathbf{Q} \mathbf{R}_A^{(2)}$ , where

$$\mathbf{Q} \equiv \mathbf{T}_{BBA} \mathbf{T}_{BBB} \mathbf{T}_{BBA}^{-1} = \gamma_B^{-1} \begin{pmatrix} E + \epsilon & -\gamma_B^2 \\ 1 & 0 \end{pmatrix}. \quad (18)$$

Therefore, we can write  $\left[ \mathbf{R}_A^{(n)}, \mathbf{R}_B^{(n)} \right]^{\text{FC}} = \left[ \mathbf{Q} \mathbf{R}_A^{(2)}, \mathbf{R}_A^{(2)} \right]^{\text{FC}} = \left[ \mathbf{Q}, \mathbf{R}_A^{(2)} \right]^{\text{FC}} \mathbf{R}_A^{(2)} = \gamma_B^{-1} \Lambda_B(E, \epsilon, \gamma_B) \tilde{\mathbf{F}}_1$ . Thus, one can establish a one-to-one correspondence between  $\text{FC}(n)$  and

precious mean based QCs of order  $n \geq 2$ , so that the zeroth-order structure of the energy spectrum of *any* FC( $n$ ) lattice essentially coincides with that corresponding to the  $n$ -label related precious mean family upon proper conjugation symmetry, as it is illustrated in Fig.7(a). Accordingly, the roots of the polynomial  $\Lambda_A(E, \epsilon, \gamma_A)$  and its conjugate  $\Lambda_B(E, \epsilon, \gamma_B)$  play a very fundamental role in the energy spectrum structure of this broad family of QCs.

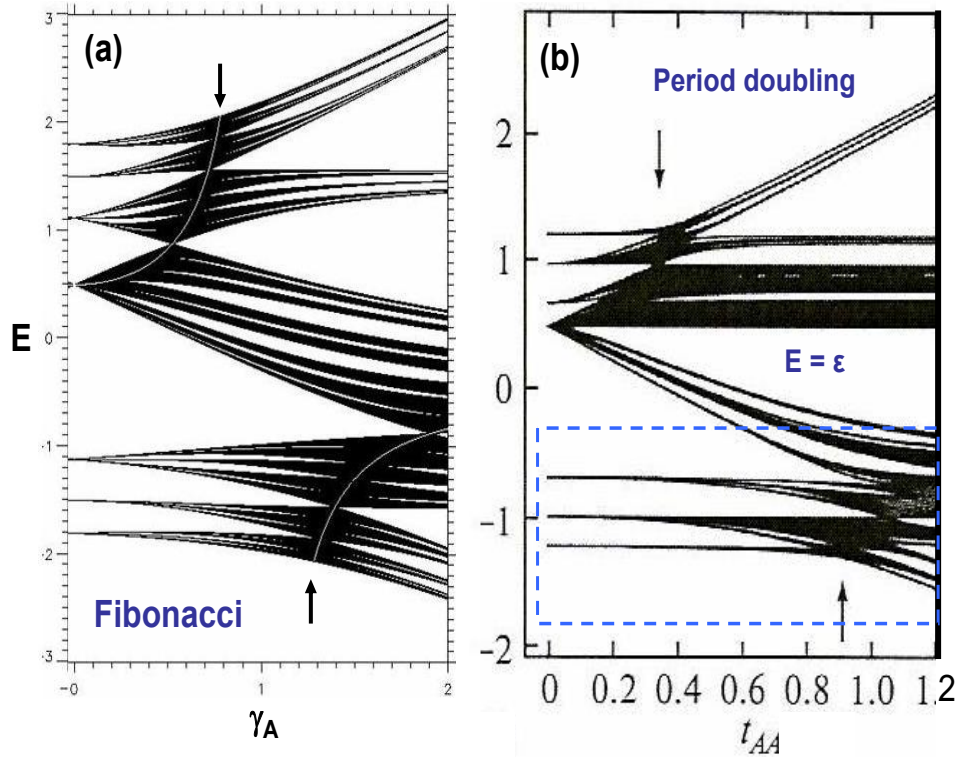
### Period doubling limit-periodic crystal

The introduction of the so-called period doubling sequence originated in the theory of dynamical systems. It describes the behavior of any system at the accumulation point of a period doubling cascade.[49] This sequence provides an example of substitution rule with an integer inflation multiplier ( $\mu_+ = 2$ ) which has an underlying limit-periodic structure instead of a quasiperiodic one. Indeed, this sequence is non-Pisot and  $|\det \mathbf{S}| \neq 1$ , hence it belongs to the  $\Pi_{\text{III}}$  class (see Table I).

Making use of the elemental block matrices listed in Table II for the period doubling based BAC, we obtain

$$[\mathbf{R}_A, \mathbf{R}_B] = \gamma_A^{-2} \Lambda_A(E, \epsilon, \gamma_A) P_3(E, \epsilon, \gamma_A) \begin{pmatrix} -1 & E + \epsilon \\ 0 & 1 \end{pmatrix}, \quad (19)$$

where  $P_3(E, \epsilon, \gamma_A) \equiv (E - \epsilon)(E^2 - \epsilon^2 - 2)$ . As we see, the commutator exhibits the characteristic algebraic structure consisting of an energy dependent polynomial factor multiplying a null trace matrix but, in this case, the degree of the polynomial is four, instead of the first degree polynomials we obtained in the study of both precious means and Fibonacci-class based QCs. In addition, we realize that this fourth degree polynomial can be decomposed in three contributing factors, one of them given by  $\Lambda_A(E, \epsilon, \gamma_A)$ . Accordingly, the zeroth-order energy spectrum of the period doubling BAC can be regarded as a superposition of the spectrum corresponding to the standard Fibonacci QC, given by the  $\Lambda_A(E, \epsilon, \gamma_A)$  polynomial root, plus the additional resonance energies  $E_0 = \epsilon$  and  $E_{\pm} = \pm\sqrt{\epsilon^2 + 2}$ , as it is shown in Fig.7(b). The energies  $E_0$  and  $E_{\pm}$  are given by molecular levels of the  $ABA$  clusters present in the chain, and they do not depend on the bond strength  $\gamma_A$ . Thus, the higher order of the polynomial factor appearing in the period doubling based BAC commutator, naturally leads to an energy spectrum exhibiting a *richer* zeroth-order structure than that previously obtained for representatives of the  $\Pi_{\text{I}}$  spectral class.



Macia.pdf

FIG. 8: Comparison between the numerically obtained phase diagrams of (a) a standard Fibonacci QC with  $N = 34$ ,  $t_{AB} = 1$ , and  $\epsilon = 0.5$  over the bond strength range  $0 \leq \gamma_A \leq 2$ , and (b) a period doubling BAC with  $N = 256$ ,  $t_{AB} = 0.6$  and  $\epsilon = 0.5$  over the same bond strength range (adapted from Ref.[50]). The vertical arrows in the period doubling diagram indicate the positions of the resonance energy curve  $E_*(\epsilon, \gamma_A)$  ends given by the  $\Lambda_A = 0$  condition, which are highlighted with a thin white line in the Fibonacci phase diagram. Note that the energy units in (b) must be scaled up by a  $5/3$  factor in order to compare with the spectral features shown in (a).

This feature is further illustrated in Fig.8, where we see that Fibonacci QC and period doubling limit-periodic crystal phase diagrams exhibit a close resemblance over the broad energy window below about  $E \simeq -0.5$  (boxed frame in Fig.8(b)), but when we consider higher energies, approaching the resonance energy  $E_0 = \epsilon = 0.5$ , both spectra significantly differ. In particular, one can readily appreciate a relatively broad, nearly straight horizontal band related to this resonance energy in the period doubling spectrum, which is completely absent in the Fibonacci one. Significant differences between both spectra can also be appre-

ciated close to the  $ABA$  cluster resonance energy value  $E_+ = 0.9$ , where one can observe the presence of a similar straight band in the period doubling spectrum.

### Copper and Nickel means based aperiodic crystals

Let us now consider the family of BACs based on metallic means sequences, which are obtained by the application of the substitution rule  $g(A) = AB^m$ ,  $g(B) = A$  (see Table I). In these sequences there are no  $B$  isolated atoms, but they always appear in clusters composed of  $m$  atoms, while  $A$  atoms can appear either isolated or forming clusters containing  $m + 1$  atoms each (see Fig.4). Their substitution matrices eigenvalues read  $\mu_{\pm} = (1 \pm \sqrt{1 + 4m})/2$  and  $|\det \mathbf{S}| = m$  (see Table I), so that the representatives of this family satisfies neither the Pisot property nor the unimodularity condition. In addition it has been recently pointed out that metallic mean sequences must be properly divided into two separate classes depending on whether the above eigenvalues take on integer values (or not), which precisely happens for  $m = \ell(\ell + 1)$  with  $\ell \in \mathbb{N}$ , giving  $\mu_+ = \ell + 1 > 1$  and  $\mu_- = -\ell$ , so that  $|\mu_-| \geq 1$ . In this case, it has been rigorously proven that their Fourier measure is pure point. For all remaining cases the pure point part of the diffraction spectrum consists of the trivial Bragg peak at zero frequency, while the remainder of the spectrum is singular continuous.[51] Accordingly, the first member of the metallic means family, the so-called copper mean (with  $m = 2$  and  $\ell = 1$ ), belongs to the limit-periodic  $\Pi_{\text{III}}$  class, whereas the next member, generally referred to as the nickel mean ( $m = 3$ ), belongs to the  $\Gamma$  class (see Fig.1 top panel).

Making use of the elemental block matrix definitions listed in Table II for the copper mean we obtain

$$\left[ \mathbf{R}_A^{(2)}, \mathbf{R}_B^{(2)} \right]^C = (\gamma_A \gamma_B)^{-2} \Lambda_{AB}^C(E) (E - \epsilon) \begin{pmatrix} -\alpha_B & 1 \\ \gamma_B^2 - \alpha_B^2 & \alpha_B \end{pmatrix}, \quad (20)$$

where

$$\Lambda_{AB}^C(E, \epsilon, \gamma_A, \gamma_B) \equiv (1 - \gamma_A^2) E^2 - 2\epsilon \gamma_A^2 E - (1 + \gamma_A^2) \epsilon^2 + \gamma_A^2 \gamma_B^2 - 1, \quad (21)$$

is a second degree polynomial in energy. As we see, the resulting degree of the commutator polynomial factor for the copper mean BAC is three, one order lower than that obtained for the period doubling BAC polynomial factor, but two orders higher than those corresponding to both precious means and Fibonacci-class QCs related commutators. From Eq.(20) we also

see that the resonance energy  $E_0 = \epsilon$ , which we previously found in the period doubling BAC energy spectrum, is also present in the copper mean one. By inspecting Eq.(21) we note that it depends on both  $A - A$  and  $B - B$  bond strength parameters, at variance with the previously considered BACs, although  $\gamma_B$  only appears in the independent term of Eq.(21), whereas  $\gamma_A$  appears in all of the polynomial coefficients instead. The  $\Lambda_{AB}^C$  polynomial roots read

$$E_{\pm}^C = \frac{\gamma_A^2 \epsilon \pm \sqrt{\epsilon^2 + (1 - \gamma_A^2)(1 - \gamma_A^2 \gamma_B^2)}}{1 - \gamma_A^2}, \quad (22)$$

so that, by equating Eqs.(11) and (22), we readily check that the resonance energy  $E_*$  only belongs to the zeroth-order energy spectrum of the copper BAC in the particular case  $\gamma_B = \gamma_A^{-1}$ . In this case, the polynomial  $\Lambda_{AB}^C$  can be factorized in the form  $\Lambda_{AB}^C = (1 - \gamma_A^2)(E + \epsilon)(E - E_*)$ . Therefore, the resonance energy  $E_*$  present in the energy spectra of both the precious means and Fibonacci-class QCs, is also present in the copper mean limit-periodic crystal spectrum when the bonds strengths satisfy the relationship  $t_{AA}t_{BB} = 1$ . The zeroth-order energy spectrum corresponding to this particular case is shown in Fig.7(c). For other choices of the  $B - B$  bond strength value we obtain more featured phase diagrams, such as those shown in Fig.9(a)-(b) for the sake of illustration. We note the presence of two curves which are located close to those corresponding to the  $E_*$  resonance energy, exhibiting a similar qualitative behavior.

Let us now consider the nickel mean based BAC. Making use of the corresponding elemental block matrix definitions listed in Table II we obtain

$$\left[ \mathbf{R}_A^{(3)}, \mathbf{R}_B^{(3)} \right]^N = \gamma_A^{-3} \gamma_B^{-4} \Lambda_{AB}^N(E) \left[ (\gamma_A^2 - (E - \epsilon))^2 \right] \begin{pmatrix} \alpha_B^2 - \gamma_B^2 & -\alpha_B \\ \alpha_B(\alpha_B^2 - 2\gamma_B^2) & \gamma_B^2 - \alpha_B^2 \end{pmatrix}, \quad (23)$$

where

$$\Lambda_{AB}^N(E, \epsilon, \gamma_A, \gamma_B) \equiv (1 - \gamma_A^2) E^3 + (1 - 3\gamma_A^2) \epsilon E^2 - rE - \epsilon q, \quad (24)$$

with  $r \equiv \epsilon^2(1 + 3\gamma_A^2) + \gamma_B^2(1 - 2\gamma_A^2) + 1$ , and  $q \equiv \epsilon^2(1 + \gamma_A^2) - \gamma_B^2(1 + 2\gamma_A^2) + 1$ , is a third degree polynomial in energy. As we see, the degree of the commutator polynomial factor is one order higher than that obtained for the period doubling BAC, two orders higher than that obtained for the copper mean BAC, and four orders higher than those corresponding to both precious means and Fibonacci-class QCs commutator polynomial factors, respectively. The polynomial  $\Lambda_{AB}^N$  can also be factorized in the particular case  $\gamma_B = \gamma_A^{-1}$  to adopt the

simpler form  $\Lambda_{AB}^N = (1 - \gamma_A^2)(E - E_*)(\alpha_B^2 - \gamma_A^{-2})$ . Accordingly, the resonance energy  $E_*$  also belongs to the nickel mean limit-periodic crystal zeroth-order energy spectrum in this case. In fact, by imposing the condition  $\Lambda_{AB}^N(E_*) \equiv 0$ , it can be shown that  $E_*$  belongs to the spectrum of the nickel mean based BAC iff  $\gamma_A = \pm\gamma_B^{-1}$ . In Fig.7(d) we show the phase diagram for the case  $\gamma_B = \gamma_A^{-1}$ , which is characterized by the presence of six main spectral features related to the resonance energies  $E = E_*$  (in black),  $E_{\pm}^{\alpha} = -\epsilon \pm \gamma_A^{-1}$  (in green), and  $E_{\pm}^{\beta} = \epsilon \pm \gamma_A$  (in purple). We see that three of these curves intersect each other at two points whose coordinates read  $(\tau^{\mp 1}, \pm(\tau - \frac{1}{2}))$ , where  $\tau$  is the golden mean.

### Mixed mean limit-quasiperiodic crystal

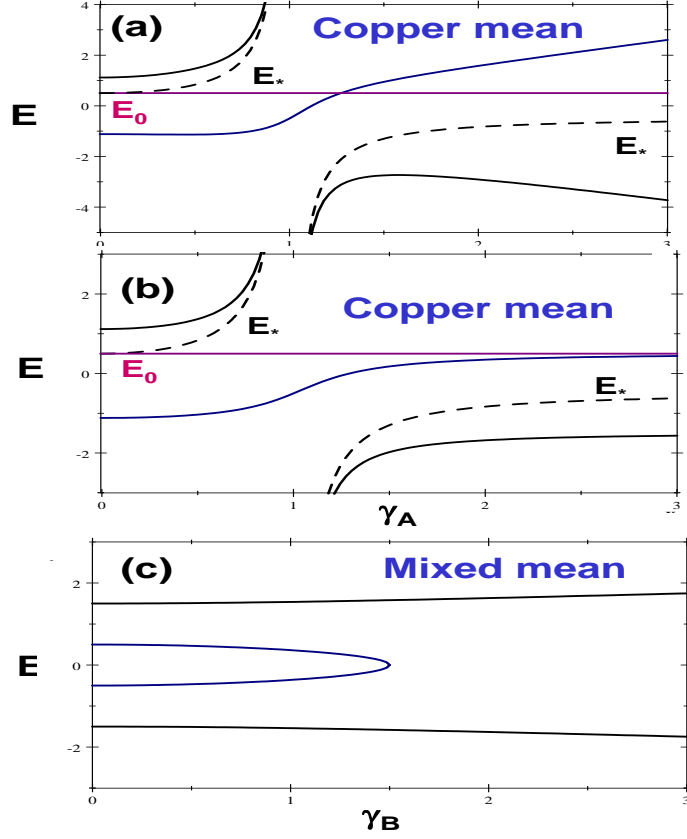
As a final example let us now consider the simplest representative of the  $\Pi_{II}$  spectral class, which belongs to the mixed mean based BACs family, and is obtained from the application of the substitution rule  $g(A) = A^n B^m$ ,  $g(B) = A$  with  $n = m = 2$  (see Table I). In this sequence there are not isolated atoms at all: the  $A$  atoms appear grouped in dimers or tetramers, whereas the  $B$  atoms always form dimers (see Fig.5(a)). Making use of the elemental block matrix definitions listed in Table II we obtain  $[\mathbf{R}_A^{(2,2)}, \mathbf{R}_B^{(2,2)}] = (\gamma_A \gamma_B)^{-1} \Lambda_{AB}^X(E, \epsilon, \gamma_A, \gamma_B) \sigma_x$ , where

$$\Lambda_{AB}^X \equiv \alpha_A^2(\alpha_B^2 - 1)(\gamma_A^{-1} - 1) - \alpha_B^2 + \alpha_A \alpha_B \gamma_A \gamma_B (2 - \gamma_A^{-1}) - \gamma_A^2 \gamma_B^2 + 1, \quad (25)$$

is a fourth degree polynomial in energy; the same degree we obtained for the period doubling BAC commutator.

We note that Eq.(25) is invariant upon the simultaneous transformation  $\alpha_A \rightarrow -\alpha_A$  and  $\alpha_B \rightarrow -\alpha_B$ , related to the energy sign change  $E \rightarrow -E$  and  $\epsilon \rightarrow -\epsilon$ . Consequently, the considered mixed mean energy spectrum will exhibit reflection symmetry with respect to the abscissas axis. By imposing the condition  $\Lambda_{AB}^X(E_*) \equiv 0$ , it can be shown that  $E_*$  belongs to the spectrum *if*  $\gamma_B = \pm\gamma_A^{-1}$  and  $\epsilon = \pm \frac{1-\gamma_A^2}{2\gamma_A} \sqrt{2 + \gamma_A^2 + \gamma_A^{-1}}$  *only*. For the sake of illustration, in Fig.9(c) we plot the phase diagram for this limit-quasiperiodic crystal for the particular case  $\gamma_A = \epsilon = 1/2$ .





Macia.pdf

FIG. 9: Phase diagrams showing the analytical zeroth-order spectra of the copper mean limit periodic crystals for (a)  $\gamma_B = 1$ , and (b)  $\gamma_B = \gamma_A$ . For the sake of comparison the curves for the resonance energy  $E_*$  (which does not belong to the spectrum) are also plotted (dashed lines). In (c) we plot the analytical phase diagram for the mixed mean  $n = m = 2$  based limit-quasiperiodic crystal with  $\gamma_A = \epsilon = 1/2$ .

## TRANSPORT PROPERTIES OF RESONANT STATES

The transport properties of the resonant electronic states given by Eq.(11) in a given BAC can be studied by means of the Landauer conductance, given by the expression  $g_N(E_*) = g_0 T_N(E_*)$ , where  $g_0 = 2e^2/h$  is the quantum of conductance, and

$$T_N(E_*) = \frac{4(\det \mathcal{M}_N)^2 \sin^2 \kappa}{[M_{12} - M_{21} + (M_{11} - M_{22}) \cos \kappa]^2 + (M_{11} + M_{22})^2 \sin^2 \kappa}, \quad (26)$$

is the transmission coefficient for a chain containing  $N$  atoms, where  $M_{ij}$  are the global transfer matrix elements.[52] In obtaining Eq.(26) one assumes the BAC is sandwiched between two periodic chains (playing the role of contacts), each one with on-site energy  $\epsilon'$

and transfer integral  $t'$ , so that their dispersion relation is given by  $E = \epsilon' + 2t' \cos \kappa$ .

In the case of a Fibonacci QC, by plugging the  $M_{ij}$  elements given by Eq.(12), into Eq.(26) we obtain

$$T_{N_1}^{(1)}(E_*) = \left[ 1 + \frac{(1 - \gamma_A^2)^2}{(4 - E_*^2)\gamma_A^2} \sin^2(N_1\phi) \right]^{-1}, \quad (27)$$

where  $\phi = \cos^{-1}(q/2)$ ,  $N_1$  is a Fibonacci number, and we have assumed  $\epsilon' = 0$  and  $t' = 1$  for the sake of simplicity. Two important conclusions can be drawn from this expression. In the first place, the transmission coefficient is always bounded below (i.e.,  $T_{N_1}^{(1)}(E_*) \neq 0$ ) for *any* lattice length, which proves the physically extended character of  $E_*$  states. In the second place, since  $\gamma_A \neq 1$  by definition, these resonant states will verify the transparency (full transmission) condition  $T_{N_1}^{(1)}(E_*) = 1$  only for those model parameters choices satisfying the relationship

$$\epsilon = \pm \frac{1 - \gamma_A^2}{\gamma_A} \cos\left(\frac{\ell\pi}{N_1}\right), \quad (28)$$

where  $\ell$  is an integer. Accordingly, most  $E_*$  resonant states in the energy spectrum show a great diversity of possible Landauer conductance values, which can take on either low or high values depending on the adopted model parameters, at variance with the highly conductive Bloch states found in periodic systems. In particular, the variation of the Landauer conductance as a function of the chemical bonding strength parameter  $\gamma_A$  agrees with the reported sensitivity of the electrical transport properties of most icosahedral quasicrystalline alloys to different stoichiometric compositions.[53]

The above well-known results concerning  $E_*$  resonant states belonging to the Fibonacci QC spectrum,[10, 42] can be properly extended to all members of the precious means based BACs family. As a suitable example, let us start with the silver mean based QC. In this case, the global transfer matrix, evaluated at the resonance energy  $E_*$ , can be expressed as  $\mathcal{M}_{N_2}^{(2)}(E_*) \equiv \left[ \mathbf{R}_A^{(2)}(E_*) \right]^l \left[ \mathbf{R}_B^{(2)}(E_*) \right]^k$ , where  $l$  and  $k$  are the numbers of  $\mathbf{R}_A^{(2)}$  and  $\mathbf{R}_B^{(2)}$  blocks, respectively. In order to explicitly calculate these power matrices we will rewrite  $\mathbf{R}_A^{(2)}$  in the general form  $\mathbf{R}_A^{(2)} = \mathbf{T}_{AAB}^{-1} \mathbf{R}_A^{(1)} \mathbf{T}_{AAB}$ , relating the corresponding elemental block matrices in the silver mean and Fibonacci QCs (compare the first two rows in Table II). On the other hand, we can express,[54]

$$\mathbf{R}_A^{(1)}(E_*) = \begin{pmatrix} q & -\gamma_A \\ \gamma_A^{-1} & 0 \end{pmatrix}^3 = \begin{pmatrix} U_3(x) & -\gamma_A U_2(x) \\ \gamma_A^{-1} U_2(x) & -U_1(x) \end{pmatrix}, \quad (29)$$

where  $x \equiv q/2 = \epsilon\gamma_A(1 - \gamma_A^2)^{-1}$ , and we have used the Cayley-Hamilton theorem. Now, we can use Eq.(6) in  $\mathbf{R}_A^{(2)} = \mathbf{T}_{AAB}^{-1}\mathbf{R}_A^{(1)}\mathbf{T}_{AAB}$ , along with the Cayley-Hamilton theorem, to obtain

$$\left[\mathbf{R}_A^{(2)}(E_*)\right]^l = \begin{pmatrix} U_l(y) + U_1(x)U_{l-1}(y) & -U_2(x)U_{l-1}(y) \\ U_2(x)U_{l-1}(y) & -U_1(x)U_{l-1}(y) - U_{l-2}(y) \end{pmatrix} = \begin{pmatrix} U_{3l}(x) & -U_{3l-1}(x) \\ U_{3l-1}(x) & -U_{3l-2}(x) \end{pmatrix}, \quad (30)$$

where  $y \equiv \frac{1}{2}\text{tr}(\mathbf{R}_A^{(2)}(E_*)) = (U_3(x) - U_1(x))/2 = T_3(x)$ , and we have used the functional relations  $U_{n-1}[T_m(x)]U_{m-1}(x) = U_{mn-1}(x)$  and  $T_m[T_n(x)] = T_{mn}(x)$ , along with the relationship  $T_n = xU_n - U_{n-2} = U_n - xU_{n-1}$ . In addition, we have

$$\left[\mathbf{R}_B^{(2)}(E_*)\right]^k = [\mathbf{T}_{AAA}(E_*)]^k = \begin{pmatrix} U_k(x) & -U_{k-1}(x) \\ U_{k-1}(x) & -U_{k-2}(x) \end{pmatrix}. \quad (31)$$

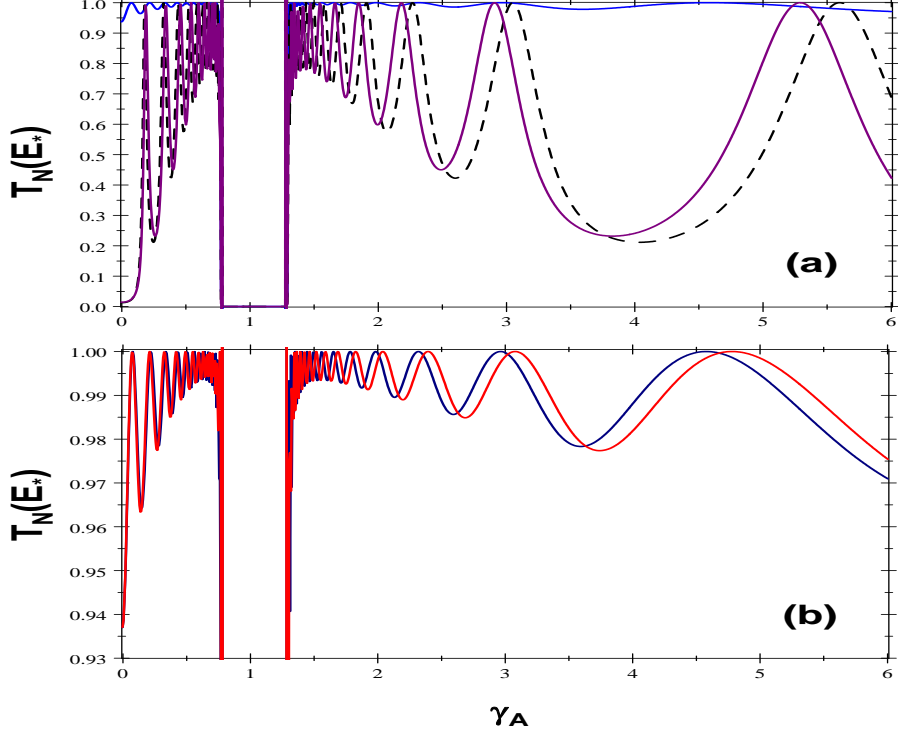
Thus, multiplying Eqs.(30) and (31), and then plugging the resulting  $\mathcal{M}_N^{(2)}(E_*)$  matrix elements into Eq.(26), using the multiplication formula  $U_{m-1}U_{n-1} = (1 - x^2)^{-1}(T_{m-n} - T_{m+n})/2$ , we finally obtain the closed expression

$$T_{N_2}^{(2)}(E_*) = \left[1 + \frac{(\gamma_A - 1)^4 E_*^2}{(4 - E_*^2)[(1 + \gamma_A^2)^2 - \gamma_A^2 E_*^2]} \sin^2(N_2\phi)\right]^{-1}, \quad (32)$$

where  $N_2$  is the number of atoms in the silver mean QC.

By following an analogous procedure we can obtain the resonance energy transmission coefficient for any precious mean based BAC with  $n > 2$  in the corresponding substitution rule (see Table II), and the obtained expressions exactly coincide with that given by Eq.(32) by just replacing  $N_2$  by the corresponding number of atoms in the considered BAC lattice. Proceeding in a similar way, we have also obtained the resonance energy transmission coefficient for the period doubling based BAC, which has the same functional form as that given by Eq.(27) for the Fibonacci QC, this time replacing the Fibonacci number  $N_1$  by the corresponding number of atoms in the considered period doubling lattice.

Accordingly, we conclude that the transmission coefficient is always bounded below (i.e.,  $T_N(E_*) \neq 0$ ) for *any* lattice length for the resonant state  $E_*$  shared by all these BACs representatives, thereby analytically confirming the physically extended character of this resonance state in a broad class of aperiodic systems. At this point, we must highlight that by extended we mean non-localized, and we do not necessarily have in mind a transparent, highly conductive state, as it occurs for Bloch states in periodic lattices. In fact, by



Macia.pdf

FIG. 10: Transmission coefficient for the resonance energy  $E_*$  as a function of the bond strength parameter  $\gamma_A$  for (a) Fibonacci (dashed), silver mean (blue), and period doubling (purple) based BACs with  $N = 34$ ,  $N = 41$ , and  $N = 32$  atoms, respectively; (b) silver (blue) and bronze (red) means based BACs with  $N = 41$  and  $N = 43$  atoms, respectively. We have adopted the value  $\epsilon = 1/2$  for the on-site energies in all the considered systems. The contacts tight-binding parameters are  $\epsilon' = 0$  and  $t' = 1$ .

systematically varying the adopted bond strength value along the path given by the curves  $\pm E_*(\epsilon, \gamma_A)$  in the phase diagram, the resulting transmission coefficients exhibit a series of alternating maxima (describing full transmission states with  $T_N(E_*) = 1$ ) and minima (taking on values within the range  $0 < T_N^{\min} < 1$ ), which correspond to those model parameters satisfying the conditions  $\sin(N\phi) = 0$  and  $\sin(N\phi) = 1$ , respectively. For any other choice of the model parameters, the transmission coefficient will adopt a value comprised within the interval  $T_N^{\min} \leq T \leq 1$ . Thus, the nature of the extended states related to the resonant energy  $E_*$  in the considered BACs does not only include transparent states, typical of periodic systems, but also embraces a big set of states exhibiting a broad palette of possible

Landauer conductance values, ranging from highly conductive to highly resistive ones.

For the sake of illustration in Fig.10 we plot the resonance energy transmission coefficients corresponding to four representative BACs as a function of the  $\gamma_A$  value for  $\epsilon = 1/2$ . In the first place, we note the presence of two separate regions, arising from the condition  $|E_*| \leq 2$ , and corresponding to the intervals  $0 \leq \gamma_A \leq \sqrt{3/5}$  and  $\gamma_A \geq \sqrt{5/3}$ , which are respectively related to the  $E_* > 0$  and  $E_* < 0$  values in the zeroth-order energy spectrum (see Figs.6-8). Within each allowed interval  $T_N(E_*)$  displays a characteristic succession of maxima and minima, as prescribed by Eqs.(27) and (32). Attending to the values attained by the transmission coefficient minima we can distinguish two main classes of BACs. Thus, resonant states corresponding to Fibonacci and period doubling BACs exhibit very similar trends, characterized by the presence of certain  $\gamma_A$  values supporting full transparent states, alternating with  $\gamma_A$  values where the transmission coefficients take on significantly small values (see Fig.10(a)). In addition, the transmission coefficient minima exhibit progressively decreasing values as we approach the limits  $\gamma_A \rightarrow 0$  and  $\gamma_A \rightarrow \infty$ , which tend to either  $T_N^{\min} = \frac{4-\epsilon^2}{4+\epsilon^2(N^2-1)}$  or  $T_N^{\min} = 0$ , depending on whether the number of atoms in the chain is even or odd, respectively. These two limits respectively describe the physical situation when one of the two types of chemical bonds, i.e.,  $A-A$  or  $A-B$ , has a bonding strength which is negligible with respect to the other, so that the original lattice can be regarded as effectively decoupled in terms of a series of atomic clusters. This physical configuration naturally leads to the presence of a number of resonant states, directly related to the corresponding clusters, namely,  $ABA$  (with molecular energy levels  $E_0 = \epsilon$ ,  $E_{\pm} = \pm\sqrt{\epsilon^2 + 2}$ ) and  $ABABA$  (with molecular energy levels  $E_0 = \epsilon$ ,  $E = \pm\sqrt{\epsilon^2 + 3}$ ,  $E = \pm\sqrt{\epsilon^2 + 1}$ ) in Fibonacci QCs (see Fig.3) or  $ABA$  and  $ABABABA$  (with molecular energy levels  $E_0 = \epsilon$ ,  $E_{\pm} = \pm\sqrt{\epsilon^2 + 2}$ ,  $E = \pm\sqrt{\epsilon^2 \pm \sqrt{2} + 2}$ ) in period doubling BACs (see Fig.4). We note that the presence of the common molecular energy level  $E_0 = \epsilon$  in all the resulting atomic clusters guarantees the existence of a marginally conductive state in the  $\gamma \rightarrow 0$  limit for all these BACs with an even number of constituent atoms.

A similar alternating behavior can be also appreciated in the transmission coefficient corresponding to precious means based BACs, such as the silver and bronze means shown in Fig.10(b), but in these systems the minima take on significantly higher values. In fact,

after Eq.(32) we get the limits

$$\lim_{\gamma \rightarrow 0} T_N^{\min}(\epsilon, \gamma) = \lim_{\gamma \rightarrow \infty} T_N^{\min}(\epsilon, \gamma) = 1 - \left(\frac{\epsilon}{2}\right)^2,$$

which are independent of the chain length and, at variance with the limits previously obtained for the Fibonacci and period doubling BACs, can take on values significantly close to the unity, hence indicating a much more conductive nature for the resonant state  $E_*$  in this case. This physical property can be traced back to the different atomic cluster structure underlying both kinds of BACs. In fact, whereas precious mean based BACs display progressively longer  $A^n$  clusters as we increase the substitution sequence generation index  $n$  (see Fig.3 and Table III), the Fibonacci and period doubling BACs only have  $AA$  dimers and  $AAA$  trimers, respectively (see Figs.3-4 and Table III). Accordingly, the resonance effects stemming from the presence of  $T_{AAA}$  local transfer matrices in the silver and bronze BACs accounts for their significantly improved transport properties.

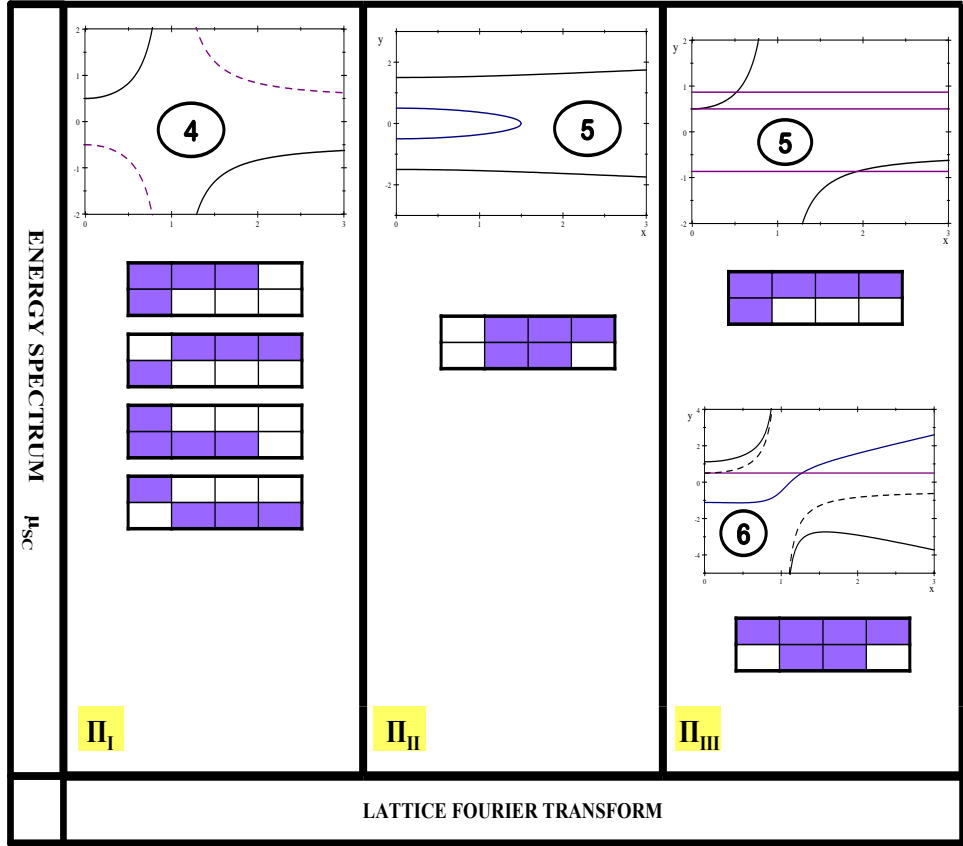
## CONCLUSIONS

Broadly speaking, symmetries present in ordered matter structures can be considered at two different spatial scales, namely, local scale symmetries describing short-range order related properties and global scale symmetries describing long-range order related properties. In the case of periodic lattices the transition from local scale to global scale features is provided by the unit cell structure. In the case of aperiodic lattices, however, the very notion of unit cell is ill-defined, so that a clear distinction between local and global scale related symmetries cannot be given in an analogous way. This shortcoming has spurred the interest in addressing some fundamental aspects regarding the relationship between global and local symmetries in both periodic and aperiodic one-dimensional systems.[55] These studies have properly highlighted the importance of considering local structure features progressively extending on successive spatial scales in order to properly describe electronic, optical, or acoustic transport properties in aperiodic systems.[56] In the present work we further elaborate along this line of thought by focusing on two characteristic symmetries shared by all aperiodic lattices based on primitive substitution rules, namely, the inflation/deflation operation describing their global scale-invariance symmetry and the repetitiveness property stemming from their local isomorphism symmetry. To properly capture bonding effects it is

necessary to consider general Hamiltonians including both diagonal and off-diagonal terms aperiodically distributed. In this way, the resulting energy spectrum structure will properly display the chemical correlation effects stemming from the long-range order present in the underlying lattice of general BACs. To this end, we have exploited an algebraic approach based on the systematic use of commutators involving block matrices related to certain atomic clusters in order to disclose a number of resonant energies stemming from locally symmetric arrangements of atoms.

In fact, by inspecting Figs.7 and 9 we realize that the resonant energy  $E_*$ , given by Eq.(11), is common to the spectrum of different BACs, namely, all the precious means QCs (including the Fibonacci QC), the period doubling limit-periodic crystal, and the Fibonacci-class QCs representatives (whose resonant energy is the conjugate of  $E_*$ ). On the contrary, this resonant energy is lacking in the energy spectrum of the considered mixed mean limit-quasiperiodic crystal representative as well as in the spectra of both copper and nickel BACs in the general case, and it only appears in the former when the bonds between  $A - A$  and  $B - B$  atoms obey the reciprocal symmetry relationship  $\gamma_B = \gamma_A^{-1}$ . This result provides an illustrative instance of a topological invariance which is shared by all of the BACs belonging to the first group, that is,  $B$  atoms always appear isolated in both precious means and period doubling based BACs (alternatively,  $A$  atoms always appear isolated in Fibonacci-class QCs), as it is indicated in the last column of Table III, and can be readily seen in Figs.3-5. This topological constraint naturally leads to the emergence of a series of relatively small atomic clusters such as  $ABA$ ,  $BAB$ ,  $BAAB$ , or  $BAAAB$ , all of them exhibiting mirror symmetry with respect to the central atom. This symmetry is translated to the related local transfer matrices  $T_{ABA}$ ,  $T_{BAB}$ ,  $T_{AAB}T_{BAA}$ , or  $T_{AAB}T_{AAA}T_{BAA}$  composing the fundamental blocks listed in the second column of Table II for the afore mentioned BACs representatives. In this way, the vanishing commutator condition satisfied by the renormalized blocks is directly connected to the local mirror symmetry of the underlying atomic clusters, in agreement with the presence of a number of perfect transmission resonant states in general aperiodic systems exhibiting translation or inversion local symmetries.[57–59]

Furthermore, from the graphical summary displayed in Fig.11 we realize that those BACs sharing the resonance energy  $E_*$  in their spectra (i.e, Fibonacci, precious mean and period doubling) have in common the presence of both  $T_{AAB}$  and  $T_{BAA}$  local transfer matrices in their renormalization block matrices, whereas those BACs lacking the resonance energy  $E_*$



Macia.pdf

FIG. 11: Spectral chart portrait showing the zeroth-order energy spectra for the BACs based on the substitution sequences included in the central row of Fig.1(b). Their structural complexity degree is illustrated in terms of the number (encircled) of different local matrices (shadowed boxes) required to fully describe their topological order at the triplet scale, according to the procedure introduced in Sec.IIA (see Fig.2).

in their spectra (i.e, metallic and mixed based means) include the conjugated local transfer matrices  $T_{BBA}$  and  $T_{ABB}$  as well due to the presence of  $B-B$  bonds in addition to  $A-A$  and  $A-B$  ones. This is illustrated in the last column of Fig.11, where we compare the spectra obtained for the period doubling and copper limit-periodic crystals. Since their substitution matrices are mutually transposed they share the same characteristic polynomial (see Table I), so that one may expect they could exhibit a similar zeroth-order energy spectrum. However, we realize that the existence of bonds between  $B-B$  atoms, present in the copper BAC but missing in the period doubling one, plays a very significant role in determining the resulting energy spectrum of these BACs. In fact, by considering the degree of the factor polynomials



present in the commutators derived for the BACs considered in this work we conclude that, with the only exception of the copper BAC, there exists a direct correlation between the polynomial degree and the number of different local transfer matrices, as can be seen in the second and third columns of Table III. Notwithstanding this, since the bonding network structure cannot be directly assessed by means of diffraction experiments only, one should not expect to find a straightforward relationship between the lattice Fourier and energy (frequency) related spectral measures.

In addition to the inflation/deflation and local isomorphism symmetries which are shared by all BACs based on primitive substitution rules, certain aperiodic structures may exhibit additional ones, such as palindromic symmetry.[59–63] We recall that a word is a palindrome if it reads the same forwards and backwards, and that a symbolic sequence is called palindromic if it contains palindromes of arbitrary length.[64] A particularly relevant example of BAC exhibiting palindromic symmetry is based on the Thue-Morse sequence and it displays both Fourier lattice and energy singular continuous spectra (see Fig.1). Quite interestingly, the algebraic approach discussed in this work can also be successfully applied to this richer aperiodic system and the obtained results will be reported elsewhere.[65]

To conclude it is worth noticing that a completely analogous treatment could be readily performed in order to obtain a spectral classification of the phonon or photonic frequency spectra corresponding to acoustic or electromagnetic waves propagating through BACs. To this end, the mathematical analogy between the Schrödinger equation describing the motion of an electron under the action of a potential and the Helmholtz equation describing a monochromatic electromagnetic wave propagating in a medium with a variable refractive index profile provides a helpful tool involving basic concepts in modern optoelectronics.[66] The knowledge gained from these extensions could be of interest for the design of optimized phononic and photonic QCs.[67–69] In this regard, the presence of states with an intermediate degree of localization, as those described in the previous section, may offer a higher degree of control and tuning flexibility, leading to the possible existence of either relatively localized or significantly extended electromagnetic intensity patterns by design. In fact, the possible occurrence of these tunable optical modes in defect-free photonic QCs would be of interest for the fabrication of high quality factor resonators as well as coupled-resonator waveguides.

## ACKNOWLEDGEMENTS

I warmly thank M. Victoria Hernández for a critical reading of the manuscript.

- 
- [1] According to the proposed terms of reference by 'crystal' we mean any solid having an essentially discrete diffraction diagram, and by 'aperiodic crystal' we mean any crystal in which three-dimensional lattice periodicity can be considered to be absent. ICrU Report of the Executive Committee for 1991, *Acta Cryst. A* **48** 922 (1992).
  - [2] T. Janssen, G. Chapuis, and M. de Boissieu, *Aperiodic Crystals: From Modulated Phases to Quasicrystals* (Oxford University Press, Oxford, 2007).
  - [3] W. Steurer and S. Deloudi, *Crystallography of Quasicrystals - Concepts, Methods and Structures*, Springer Series in Materials Science 126 (Springer Verlag, Berlin, 2009).
  - [4] E. Maciá Barber, *Aperiodic Structures in Condensed Matter* (CRC Taylor & Francis, Boca Raton, 2009).
  - [5] D. Levine and P. J. Steinhardt, *Phys. Rev. Lett.* **53** 2477 (1984).
  - [6] M. Baake and U. Grimm, *Aperiodic Order I: A Mathematical Invitation*, *Encyclopedia of Mathematics and Its Applications* 149 (Cambridge University Press, Cambridge, 2013).
  - [7] U. Grimm, *Acta Cryst.* **B71**, 258 (2015).
  - [8] E. Maciá, *Rep. Prog. Phys.* **69**, 397 (2006).
  - [9] L. Dal Negro and S. V. Boriskina, *Laser Photon. Rev.* **6**, 178-218 (2012).
  - [10] E. Maciá, *ISRN Condensed Matter Physics* **2014**, 165943 (2014). doi: 10.1155/2014/165943.
  - [11] L. Dal Negro, J. Lawrence, J. Trevine, and G. Walsh, *Aperiodic order for nanophotonics*. In L. Dal Negro (Ed.), *Optics of Aperiodic Structures: Fundamentals and Device Applications* (Pan Stanford, USA, 2014). pp.1-55.
  - [12] M. Boguslawski, N. M. Lučić, F. Diebel, D. V. Timotijević, C. Denz, and D. M. Jović Savić, *Optica*, **3**, 711-717 (2016).
  - [13] L. Dal Negro, R. Wang, and A. Pinheiro, *Crystals* **6**, 161 (2016); doi:10.3390/cryst6120161
  - [14] S. Yu, X. Piao, J. Hong, and N. Park, *Sci. Adv.* 2016; **2**: e1501851.
  - [15] H. J. Changlani, N. M. Tubman, and T. L. Hughes, *Sci. Rep.* **6**: 31897 (2016); doi: 10.1038/srep31897.

- [16] Yu. Kh. Vekilov, E. I. Isaev, and S. F. Arslanov, Phys. Rev. B **62**, 14040 (2000).
- [17] Yu. Kh. Vekilov and E. I. Isaev, Phys. Lett. A **300**, 500 (2002).
- [18] A substitution rule is called primitive when all entries of its related substitution matrix power  $S^N$  are strictly positive integers (i.e.,  $s_{ij} \neq 0$ ), for some  $N \geq 1$ . This means that there exists an integer  $n$  such that for all pairs of letters  $A$  and  $B$  in  $A$  the word  $g^n(A)$  contains the letter  $B$ .
- [19] A. Bovier and J. M. Ghez, J. Phys. A: Math. Gen. **28**, 2313 (1995).
- [20] J. M. Luck, C. Godrèche, A. Janner, and T. Janssen. J. Phys. A: Math. Gen. **26**, 1951 (1993).
- [21] D. Barache and J. M. Luck, Phys. Rev. B **49**, 15004 (1994).
- [22] R. Endou, K. Niizeki and N. Fujita, J. Phys. A: Math. Gen. **37**, L151 (2004).
- [23] K. Niizeki, and N. Fujita, J. Phys. Soc. Jpn. **71**, 99 (2002).
- [24] M. Kolář, Phys. Rev. B **47**, 5489 (1993).
- [25] M. Kolář, B. Iochum, and L. Raymond, J. Phys. A: Math. Gen. **26**, 7343 (1993).
- [26] F. Gähler and R. Klitzing, in The Mathematics of Long-Range Aperiodic Order, ed. R. V. Moody (Kluwer, Dordrecht, 1995) pp. 141-174. (Nato Science Series C: Mathematical and Physical Sciences, vol. 489).
- [27] J. E. S. Socolar and J. M. Taylor, J. Comb. Theory A **118**, 2207 (2011).
- [28] C. Marcoux and J. E. S. Socolar, Phys. Rev. B **93**, 174102 (2016).
- [29] K. Niizeki and N. Fujita, J. Phys. A: Math. Gen. **38**, L199 (2005).
- [30] Generalization to alphabets containing more than two letters straightforwardly follows.
- [31] E. Bombieri and J. E. Taylor, Contemp. Math. **64**, 241 (1987)
- [32] C. Godrèche, J. M. Luck, and F. Vallet, J. Phys. A **20**, 4483 (1987).
- [33] H. Bruin, A. Clark, and R. Fokkink, Topol. Appl. **205**, 1-3 (2016).
- [34] A Pisot-Vijayaraghavan number (also called a Pisot number for short) is a real algebraic number (i.e., a number which is obtained from the solution of an algebraic equation) greater than one, all of whose conjugate elements (the other solutions of the algebraic equation) have absolute value less than unity. If at least one of the conjugate elements equals unity then it will be referred to as a Salem number.
- [35] It is important to highlight that the Pisot property provides a necessary condition for a pure point diffraction spectrum, but it is not sufficient. For instance, the Thue-Morse sequence has the Pisot property, but it has a singular continuous Fourier spectrum.

- [36] E. L. Albuquerque and M. G. Cottam, Phys. Rep. **376**, 225 (2003).
- [37] E. L. Albuquerque and M. G. Cottam, Polaritons in Periodic and Quasiperiodic Structures (Elsevier, Amsterdam, 2004).
- [38] U. Grimm, Isr. J. Chem. **51**, 1257 (2011).
- [39] J. S. W. Lamb and F. Wijnands, J. Stat. Phys. **90**, 261 (1998).
- [40] L. Kroon and R. Riklund, J. Phys. A: Math. Gen. **36**, 4519 (2003).
- [41] To the best of my knowledge a fully-complex BAC exhibiting the eight possible local transfer matrices in the global transfer matrix  $M_N(E)$  has not yet been described in the literature. An example of periodic lattice fulfilling this condition has a unit cell containing ten atoms arranged as follows: *ABABBBAAAB*.
- [42] E. Maciá and F. Domínguez-Adame, Phys. Rev. Lett. **76**, 2957 (1996).
- [43] E. Maciá, Phys. Rev. B **60**, 10032 (1999).
- [44] X. Wang, U. Grimm and M. Schreiber, Phys. Rev. B **62**, 14020 (2000).
- [45] T. Wolf and P. Schmelcher, Phys. Rev. E **93**, 042215 (2016).
- [46] E. Maciá and R. Rodríguez-Oliveros, Phys. Rev. B **74**, 144202 (2006).
- [47] V. Kumar, J. Phys. Condens. Matt. **2**, 1349 (1990).
- [48] X. Fu, Y. Liu, P. Zhou, and W. Sritrakool, Phys. Rev. B **55**, 2882 (1997).
- [49] P. Collet and J. P. Eckmann, *Iterated Maps on the Interval as Dynamical Systems* (Birkhäuser, Boston, 1980).
- [50] P. Yu. Korotaev, Yu. Kh. Vekilov, and N. E. Kaputkina, J. Exp. Theor. Phys. **118**, 304 (2014).
- [51] M. Baake and U. Grimm, J. Phys. Conf. Series **809**, 012026 (2017).
- [52] D. Sánchez, V. Sánchez, and C. Wang, J. Non-Cryst. Solids, 450, 194 (2016).
- [53] J. M. Dubois, *Useful Quasicrystals* (World Scientific, Singapore, 2005).
- [54] G. J. Jin and Z. D. Wang, Phys. Rev. Lett. **79**, 5298 (1997).
- [55] P. A. Kalozoumis, C. Morfonios, F. K. Diakonov, and P. Schmelcher, Phys. Rev. Lett. **113**, 050403 (2014).
- [56] P. A. Kalozoumis, O. Richoux, F. K. Diakonov, G. Theocharis, and P. Schmelcher, Phys. Rev. B **92**, 014303 (2015).
- [57] P. A. Kalozoumis, C. Morfonios, F. K. Diakonov, and P. Schmelcher, Phys. Rev. B **87**, 032113 (2013).
- [58] P. A. Kalozoumis, C. Morfonios, N. Palaiodimopoulos, F. K. Diakonov, and P. Schmelcher,

- Phys. Rev. B **88**, 033857 (2013).
- [59] C. Morfonios, P. Schmelcher, P. A. Kaloizoumis, and F. K. Diakonov, Nonlinear. Dyn. **78**, 71 (2014).
  - [60] A. Hof, O. Knill, and B. Simon, Comm. Math. Phys. **174**, 149 (1995).
  - [61] M. Baake, Lett. Math. Phys. **49**, 217 (1999).
  - [62] J. P. Allouche, M. Baake, J. Cassaigne, and D. Damanik, Theoret. Comput. Sci. **292**, 9 (2003).
  - [63] S. Labbé and E. Pelantová, Eur. J. Combin. **51**, 200 (2016).
  - [64] A well-known counter-example is the Rudin-Shapiro sequence which only contains palindromes of length 1-8, 10, 12 and 14, as discussed in J. P. Allouche, J. Math. Phys. **38**, 1843 (1997).
  - [65] E. Maciá (unpublished).
  - [66] S.V. Gaponenko, *Introduction to Nanophotonics* (Cambridge University Press, Cambridge, 2010).
  - [67] E. Maciá, Rep. Prog. Phys. **75**, 036502 (2012).
  - [68] L. Dal Negro, (Ed.), *Optics of Aperiodic Structures: Fundamentals and Device Applications*, (Pan Stanford Publishing Pte. Ltd., Singapore, 2014).
  - [69] E. Maciá, Crystals **7**, 64 (2017); doi:10.3390/cryst7030064.

SEQUENCE	SUBSTITUTION RULE	$S$	$\det S$	EIGENVALUES	CLASS
<b>Fibonacci</b>	$g(A) = AB \quad g(B) = A$	$\begin{pmatrix} 1 & 1 \\ 1 & 0 \end{pmatrix}$	$-1$	$\mu_{\pm} = \frac{1 \pm \sqrt{5}}{2}$	$\Pi_I$
<b>Silver mean</b>	$g(A) = AAB \quad g(B) = A$	$\begin{pmatrix} 2 & 1 \\ 1 & 0 \end{pmatrix}$	$-1$	$\mu_{\pm} = 1 \pm \sqrt{2}$	$\Pi_I$
<b>Bronze mean</b>	$g(A) = AAAB \quad g(B) = A$	$\begin{pmatrix} 3 & 1 \\ 1 & 0 \end{pmatrix}$	$-1$	$\mu_{\pm} = \frac{3 \pm \sqrt{13}}{2}$	$\Pi_I$
<b>Precious means</b> $(n > 3)$	$g(A) = A^n B \quad g(B) = A$	$\begin{pmatrix} n & 1 \\ 1 & 0 \end{pmatrix}$	$-1$	$\mu_{\pm} = \frac{n \pm \sqrt{n^2 + 4}}{2}$	$\Pi_I$
<b>Fibonacci-class</b>	$g(A) = B^{n-1}AB \quad g(B) = B^{n-1}A$	$\begin{pmatrix} 1 & 1 \\ n & n-1 \end{pmatrix}$	$-1$	$\mu_{\pm} = \frac{n \pm \sqrt{n^2 + 4}}{2}$	$\Pi_I$
Period-doubling	$g(A) = AB \quad g(B) = AA$	$\begin{pmatrix} 1 & 2 \\ 1 & 0 \end{pmatrix}$	$-2$	$\mu_+ = 2 \quad \mu_- = -1$	$\Pi_{III}$
Copper mean	$g(A) = ABB \quad g(B) = A$	$\begin{pmatrix} 1 & 1 \\ 2 & 0 \end{pmatrix}$	$-2$	$\mu_+ = 2, \quad \mu_- = -1$	$\Pi_{III}$
Nickel mean	$g(A) = AB BB \quad g(B) = A$	$\begin{pmatrix} 1 & 1 \\ 3 & 0 \end{pmatrix}$	$-3$	$\mu_{\pm} = \frac{1 \pm \sqrt{13}}{2}$	$\Gamma$
Metallic means $(m = \ell(\ell + 1))$	$g(A) = AB^m \quad g(B) = A$	$\begin{pmatrix} 1 & 1 \\ m & 0 \end{pmatrix}$	$-m$	$\mu_{\pm} = \frac{1 \pm \sqrt{1+4m}}{2}$	$\Pi_{III}$
Mixed means $(n \geq m)$	$g(A) = A^n B^m \quad g(B) = A$	$\begin{pmatrix} n & 1 \\ m & 0 \end{pmatrix}$	$-m$	$\mu_{\pm} = \frac{n \pm \sqrt{n^2 + 4m}}{2}$	$\Pi_{II}$
Mixed means $(n < m)$	$g(A) = A^n B^m \quad g(B) = A$	$\begin{pmatrix} n & 1 \\ m & 0 \end{pmatrix}$	$-m$	$\mu_{\pm} = \frac{n \pm \sqrt{n^2 + 4m}}{2}$	$\Pi_{III}$
<b>Thue-Morse</b>	$g(A) = AB \quad g(B) = BA$	$\begin{pmatrix} 1 & 1 \\ 1 & 1 \end{pmatrix}$	$0$	$\mu_+ = 2, \quad \mu_- = 0$	$\Gamma$
<b>Periodic</b>	$g(A) = AB \quad g(B) = AB$	$\begin{pmatrix} 1 & 1 \\ 1 & 1 \end{pmatrix}$	$0$	$\mu_+ = 2, \quad \mu_- = 0$	$\Pi_0$

TABLE I: Substitution sequences most widely considered in the study of BACs based on the alphabet  $\{A, B\}$ , where  $n$  and  $m$  are positive integers. The corresponding substitution matrix  $S$ ,

SEQUENCE	BLOCK MATRICES	SUBSTITUTION RULE
Fibonacci ( $n = 1$ )	$R_A^{(1)} = T_{AAB}T_{BAA}T_{ABA}$ $R_B^{(1)} = T_{BAB}T_{ABA}$	$g(R_A^{(1)}) = R_A^{(1)}R_B^{(1)}$ $g(R_B^{(1)}) = R_A^{(1)}$
Silver mean ( $n = 2$ )	$R_A^{(2)} = T_{BAA}T_{ABA}T_{AAB}$ $R_B^{(2)} = T_{AAA}$	$g(R_A^{(2)}) = R_A^{(2)}R_A^{(2)}R_B^{(2)}$ $g(R_B^{(2)}) = R_A^{(2)}$
Bronze mean ( $n = 3$ )	$R_A^{(3)} = T_{BAA}T_{ABA}T_{AAB}T_{AAA}$ $R_B^{(3)} = T_{AAA}$	$g(R_A^{(3)}) = R_A^{(3)}R_A^{(3)}R_A^{(3)}R_B^{(3)}$ $g(R_B^{(3)}) = R_A^{(3)}$
Precious means ( $n > 2$ )	$R_A^{(n)} = R_A^{(n-1)}T_{AAA}$ $R_B^{(n)} = T_{AAA}$	$g(R_A^{(n)}) = \left[R_A^{(n)}\right]^n R_B^{(n)}$ $g(R_B^{(n)}) = R_A^{(n)}$
Fibonacci-class ( $n = 2$ )	$R_A^{(2)} = T_{BBA}T_{ABB}T_{BAB}$ $R_B^{(2)} = T_{ABA}T_{BAB}$	$g(R_A^{(2)}) = R_B^{(2)}R_A^{(2)}R_B^{(2)}$ $g(R_B^{(2)}) = R_B^{(2)}R_A^{(2)}$
Fibonacci-class ( $n > 2$ )	$R_A^{(n)} = T_{BBA}T_{BBB}^{n-2}T_{ABB}T_{BAB}$ $R_B^{(n)} = R_A^{(n-1)}$	$g(R_A^{(n)}) = \left[R_B^{(n)}\right]^{n-1} R_A^{(n)}R_B^{(n)}$ $g(R_B^{(n)}) = \left[R_B^{(n)}\right]^{n-1} R_A^{(n)}$
Period-doubling	$R_A = T_{ABA}T_{AAB}T_{AAA}T_{BAA}$ $R_B = T_{ABA}T_{BAB}T_{ABA}T_{BAB}$	$g(R_A) = R_AR_B$ $g(R_B) = R_AR_A$
Copper mean ( $m = 2$ )	$R_A^{(2)} = T_{AAB}T_{AAA}T_{BAA}T_{BBA}T_{ABB}$ $R_B^{(2)} = T_{BAB}T_{BBA}T_{ABB}$	$g(R_A^{(2)}) = R_A^{(2)}R_B^{(2)}R_B^{(2)}$ $g(R_B^{(2)}) = R_A^{(2)}$
Nickel mean ( $m = 3$ )	$R_A^{(3)} = T_{AAB}T_{AAA}^2T_{BAA}T_{BBA}T_{BBB}T_{ABB}$ $R_B^{(3)} = T_{BAB}T_{BBA}T_{BBB}T_{ABB}$	$g(R_A^{(3)}) = R_A^{(3)}R_B^{(3)}R_B^{(3)}R_B^{(3)}$ $g(R_B^{(3)}) = R_A^{(3)}$
Metallic means ( $m > 1$ )	$R_A^{(m)} = T_{AAB}T_{AAA}^{m-1}T_{BAA}T_{BBA}T_{BBB}^{m-2}T_{ABB}$ $R_B^{(m)} = T_{BAB}T_{BBA}T_{BBB}^{m-2}T_{ABB}$	$g(R_A^{(m)}) = R_A^{(m)}\left[R_B^{(m)}\right]^m$ $g(R_B^{(m)}) = R_A^{(m)}$
Mixed mean ( $n = m = 2$ )	$R_A^{(2,2)} = T_{AAB}T_{ABB}T_{BBA}T_{BAA}$ $R_B^{(2,2)} = T_{AAA}$	$g(R_A^{(2,2)}) = \left[R_A^{(2,2)}\right]^2\left[R_B^{(2,2)}\right]^2$ $g(R_B^{(2,2)}) = R_A^{(2,2)}$
Mixed mean ( $n = 3, m = 2$ )	$R_A^{(3,2)} = R_A^{(2,2)}T_{AAA}$ $R_B^{(3,2)} = T_{AAA}$	$g(R_A^{(3,2)}) = \left[R_A^{(3,2)}\right]^3\left[R_B^{(3,2)}\right]^2$ $g(R_B^{(3,2)}) = R_A^{(3,2)}$
Mixed mean ( $n = 2, m = 3$ )	$R_A^{(2,3)} = T_{AAB}T_{ABB}T_{BBB}T_{BBA}T_{BAA}$ $R_B^{(2,3)} = T_{AAA}$	$g(R_A^{(2,3)}) = \left[R_A^{(2,3)}\right]^2\left[R_B^{(2,3)}\right]^3$ $g(R_B^{(2,3)}) = R_A^{(2,3)}$

TABLE II: Structure of the elemental block matrices  $\mathbf{R}_A^{(n,m)}$  and  $\mathbf{R}_B^{(n,m)}$  in terms of local transfer matrices  $\mathbf{T}_{k,k\pm 1}$ , along with the related substitution rules defining the global transfer matrix  $\mathcal{M}_N(E)$  for several BACs listed in Table I. By comparing the last column with the second column of Table I it can be readily appreciated that the elemental block matrices obey exactly the same substitution rules as the atoms  $A$  and  $B$ .

SEQUENCE	$T_{k,k\pm 1}$ NUMBER	POLYNOMIAL DEGREE	CLUSTERING FEATURES
Fibonacci	4	1	Isolated $A$ and $B$ atoms; $AA$ dimers
Precious means	4	1	Isolated $B$ atoms; $A^n$ and $A^{n+1}$ clusters
Fibonacci-class	4	1	Isolated $A$ atoms; $B^{n-1}$ and $B^n$ clusters
Period-doubling	5	4	Isolated $A$ and $B$ atoms; $AAA$ triplets
Mixed mean ( $n = m = 2$ )	5	4	$BB$ and $AA$ dimers; $AAAA$ clusters
Copper mean	6	3	Isolated $A$ atoms; $BB$ dimers; $AAA$ triplets
Nickel mean	7	5	Isolated $A$ atoms; $BBB$ triplets; $AAAA$ clusters

TABLE III: Relationship among the chemical complexity of different BACs, as measured by the number of different local transfer matrices  $\mathbf{T}_{k,k\pm 1}$  present in their global transfer matrix  $\mathcal{M}_N(E)$  in terms of local transfer matrices, the degree of the energy dependent polynomial present in their corresponding commutators, and the main clusters present in their atomic lattices.